

Mixture-of-experts Wishart model for covariance matrices with an application to Cancer drug screening

The Tien Mai¹  , Zhi Zhao² 

¹Norwegian Institute of Public Health, 0456 Oslo, Norway.

²University of Oslo, 0372 Oslo, Norway.

email: the.tien.mai@fhi.no

Abstract

Covariance matrices arise naturally in different scientific fields, including finance, genomics, and neuroscience, where they encode dependence structures and reveal essential features of complex multivariate systems. In this work, we introduce a comprehensive Bayesian framework for analyzing heterogeneous covariance data through both classical mixture models and a novel mixture-of-experts Wishart (MoE–Wishart) model. The proposed MoE–Wishart model extends standard Wishart mixtures by allowing mixture weights to depend on predictors through a multinomial logistic gating network. This formulation enables the model to capture complex, nonlinear heterogeneity in covariance structures and to adapt subpopulation membership probabilities to covariate-dependent patterns. To perform inference, we develop an efficient Gibbs-within–Metropolis–Hastings sampling algorithm tailored to the geometry of the Wishart likelihood and the gating network. We additionally derive an Expectation–Maximization algorithm for maximum likelihood estimation in the mixture-of-experts setting. Extensive simulation studies demonstrate that the proposed Bayesian and maximum likelihood estimators achieve accurate subpopulation recovery and estimation under a range of heterogeneous covariance scenarios. Finally, we present an innovative application of our methodology to a challenging dataset: cancer drug sensitivity profiles, illustrating the ability of the MoE–Wishart model to leverage covariance across drug dosages and replicate measurements.

Our methods are implemented in the R package `moewishart` available at <https://github.com/zhi Zhao/moewishart>.

Keywords: Bayesian inference; MCMC; MLE; EM algorithm; covariance matrix; mixture model.

1 Introduction

In traditional statistical modeling, it is often assumed that a single, universal relationship between variables holds across an entire population. Observations that deviate from this relationship are typically treated as outliers. In practice, however, real-world systems are rarely homogeneous. Instead, data frequently arise from multiple latent subpopulations, each characterized by distinct behavioral patterns or structural relationships. As the scale and complexity of modern datasets continue to increase, it becomes essential to appropriately model such hidden heterogeneity. Mixture models [24] provide a powerful and principled framework for extending classical clustering and regression methods to settings in which population structure is intrinsically heterogeneous [5].

In general, covariance matrices play a central role in scientific inquiry, as they encode patterns of linear dependence among variables and reveal the underlying structure of multivariate phenomena. Their importance spans a wide range of application domains. In finance, covariance matrices underpin portfolio allocation, risk assessment, and investment strategies [30, 11]. In imaging/pattern recognition, covariance among pixel/voxel intensities or regions captures spatial and spatio-temporal dependencies, supporting tasks as clustering and feature extraction [32]. In genomics, quantifying gene–gene interactions may help

identify biologically meaningful trait associations [27]. In neuroscience, covariance matrices are used to characterize functional connectivity and network-level interactions between brain regions [21]. Moreover, covariance structures form the computational foundation of essential multivariate techniques such as Principal Component Analysis and Factor Analysis [26, 7].

Despite their ubiquity, covariance structures are often overlooked in standard clustering techniques. Widely used algorithms such as k-means and hierarchical clustering primarily rely on differences in mean structure, thereby ignoring potentially rich information encoded in covariance patterns. To address this limitation, recent research has increasingly focused on clustering based on covariance heterogeneity. An important probabilistic framework was introduced by [8], who proposed a mixture model with Wishart component densities and an Expectation–Maximization (EM) algorithm for parameter estimation. Subsequent extensions include sparse penalization for high-dimensional covariance estimation [3], variational Bayesian inference [21], and applications to discriminant analysis [4]. Relatedly, [6] considered finite mixtures of skewed matrix-variate distributions, including the matrix-variate variance-gamma distribution as a generalization of the Wishart, with inference carried out via EM algorithms. Despite these advances, a comprehensive fully Bayesian treatment of Wishart mixture models has received relatively limited attention.

In this paper, we address this gap by first developing a fully Bayesian formulation of the classical mixture of Wishart distributions. Building on this foundation, we introduce a novel Mixture-of-Experts Wishart (MoE–Wishart) model, which integrates the flexibility of mixture-of-experts architectures with the interpretability and structure of Wishart-distributed covariance data. Unlike standard mixture models with fixed mixing proportions, mixture-of-experts models [12] allow cluster membership probabilities to depend explicitly on covariates, thereby enabling the model to learn how latent subpopulations vary across the predictor space. Through a probabilistic gating network governed by a softmax link [23], the MoE framework partitions the input space and dynamically assigns observations to expert components. This structure allows the proposed model to capture complex, nonlinear, and piecewise behavior in covariance patterns, which is particularly valuable in high-dimensional or highly heterogeneous settings. For a general overview of mixture-of-experts models, see [20].

For posterior inference in both the mixture model and the proposed MoE–Wishart extension, we utilize efficient Markov chain Monte Carlo (MCMC) algorithms. In particular, we construct a Gibbs-within–Metropolis–Hastings sampler tailored to the geometry of the posterior distribution induced by symmetric positive definite covariance matrices. In addition, we derive an Expectation–Maximization algorithm for maximum likelihood estimation in the mixture-of-experts setting, where closed-form updates are not readily available.

The main contributions of this paper are therefore threefold: (i) a fully Bayesian formulation of the mixture of Wishart distributions, (ii) the introduction of a new mixture-of-experts model for covariance matrix data (MoE–Wishart model), and (iii) tailored inference algorithms for the MoE–Wishart model, including both MCMC and EM procedures. To facilitate reproducibility and practical adoption, we additionally provide an R package `moewishart` that implements all proposed methods (available at <https://github.com/zhizhui/moewishart>).

We conduct extensive simulation studies to assess the statistical accuracy and computational performance of the proposed methods. Finally, we illustrate their practical utility through a real-data application to study covariance patterns arising in cancer drug discovery and repurposing. In biomedicine, drug repositioning refers to finding new uses for approved and preclinical drugs [1]. With the growing availability of data from large-scale drug screens and relevant molecular information, data-driven drug repositioning has the potential to accelerate clinical advances. Specifically, exploiting drug–drug similarity or clusters based on shared molecular targets and pharmacological or chemical structures can facilitate drug repurposing [34, 9]. Drug screening data are typically derived from experiments in which individual drugs, tested at multiple dosages/concentrations, are applied to patient tissue samples or cell lines. Each drug’s efficacy is therefore assessed via cell viability measured on replicated samples across multiple dosages. Currently, most models use a scalar summarized descriptor (e.g., IC₅₀ or area under the drug dose-response curve)

to represent each drug's efficacy [28, 19, 29, 36], but this approach loses substantial information. We propose to use, for each drug, the covariance descriptor of its response data (i.e., covariance matrix of cell viability on replicated samples across multiple dosages), and then model latent clusters based on covariance matrices from many drugs. Drugs clustered in one group may indicate similar functionality and suggest new uses of some drugs.

The remainder of the paper is organized as follows. Section 2 introduces the Wishart mixture and mixture-of-experts models for covariance matrix data. Section 3 develops a Bayesian framework together with MCMC sampling algorithms for both the mixture and mixture-of-experts models. Section 4 presents an EM algorithm for obtaining maximum likelihood estimates in the mixture-of-experts model. Simulation studies are reported in Section 5 and an application to cancer drug screening data is presented in Section 6. We discuss and conclude in Section 7.

2 Mixture of covariance matrices models

We first describe the mixture model and then present extension to mixture-of-expert models.

2.1 Mixture model

Let S_1, \dots, S_n be observed symmetric positive definite (SPD) $p \times p$ matrices. We model these as a finite mixture of Wishart distributions:

$$S_i \mid z_i = k, \Sigma_k, \nu_k \stackrel{\text{ind}}{\sim} \mathcal{W}_p(\nu_k, \Sigma_k), \quad i = 1, \dots, n, \quad (1)$$

where $z_i \in \{1, \dots, K\}$ denotes the latent (unobserved) cluster label for observation i . Here, $\nu_k > p - 1$ is the degrees of freedom of the Wishart, and Σ_k is the cluster-specific scale (covariance) matrix for cluster k . The Wishart density (with our parametrization) is

$$f_{\mathcal{W}}(S \mid \nu, \Sigma) = \frac{|S|^{(\nu-p-1)/2} \exp\left(-\frac{1}{2} \text{tr}(\Sigma^{-1}S)\right)}{2^{\nu p/2} |\Sigma|^{\nu/2} \Gamma_p\left(\frac{\nu}{2}\right)}, \quad (2)$$

where $\Gamma_p(\cdot)$ is the multivariate Gamma function.

Marginalizing over the latent cluster labels z_i , the distribution of each observed matrix S_i can be written in a mixture density form. Let $\boldsymbol{\pi} = (\pi_1, \dots, \pi_K)$ denote the (fixed) mixture weights, where $\pi_k = \Pr(z_i = k)$, $\pi_k \geq 0$, and $\sum_{k=1}^K \pi_k = 1$. Then the conditional density of covariance observation S_i (marginal over the latent cluster labels z_i) is

$$f(S_i \mid \boldsymbol{\pi}, \{\Sigma_k, \nu_k\}_{k=1}^K) = \sum_{k=1}^K \pi_k f_{\mathcal{W}}(S_i \mid \nu_k, \Sigma_k), \quad i = 1, \dots, n, \quad (3)$$

where $f_{\mathcal{W}}(\cdot \mid \nu_k, \Sigma_k)$ is the Wishart density defined in (2). This formulation highlights that the population distribution of SPD matrices is represented as a convex combination of K Wishart components, each corresponding to a distinct latent cluster with its own scale matrix and degrees of freedom. Such finite mixture of Wishart distributions offers a coherent and interpretable framework for modeling heterogeneous collections of covariance matrices, while explicitly respecting their geometric and positive-definiteness constraints. By allowing both the scale matrices and degrees of freedom to vary across clusters, the model captures differences in both covariance structure and dispersion, yielding flexible yet parsimonious representations of latent subpopulations.

2.2 Mixture-of-Experts Wishart model

Let S_1, \dots, S_n be observed SPD matrices of size $p \times p$ and let $X \in \mathbb{R}^{n \times q}$ be additional covariates. We consider an extension of the mixture model in (1) to a finite mixture-of-experts (MoE) model with K Wishart experts (MoE-Wishart):

$$S_i \mid z_i = k, \Sigma_k, \nu_k \stackrel{\text{ind}}{\sim} \mathcal{W}_p(\nu_k, \Sigma_k), \\ \Pr(z_i = k \mid X_i) = \pi_{ik}, \quad \text{with } k = 1, \dots, K,$$

where the gating probabilities are multinomial logistic (softmax) functions of X_i :

$$\pi_{ik}(X_i; \beta_k) = \frac{\exp(X_i^\top \beta_k)}{\sum_{\ell=1}^K \exp(X_i^\top \beta_\ell)}, \quad \beta_K \equiv 0 \text{ (for identifiability).} \quad (4)$$

Under this MoE formulation, the conditional density of S_i given covariates X_i (marginal over the latent cluster labels z_i) is

$$f(S_i \mid X_i, \{\beta_k, \Sigma_k, \nu_k\}_{k=1}^K) = \sum_{k=1}^K \pi_{ik}(X_i; \beta) f_{\mathcal{W}}(S_i \mid \nu_k, \Sigma_k). \quad (5)$$

This MoE-Wishart model extends the baseline finite mixture formulation by explicitly incorporating covariate information into the clustering mechanism, thereby allowing cluster membership to vary systematically with observed predictors rather than being governed by fixed mixing proportions. In the literature, X_i are also called concomitant variables, so that the MoE models are also referred to as mixture models with concomitant covariates. While the previous mixture model assumes exchangeable observations with homogeneous prior cluster probabilities, the MoE formulation introduces a multinomial logistic gating network that adapts the allocation probabilities to subject-specific covariates, yielding a more flexible and interpretable representation of heterogeneity. In this setting, the Wishart experts retain their role in modeling cluster-specific covariance structure and dispersion through (Σ_k, ν_k) , but the inclusion of X_i enables the model to capture covariate-driven shifts in latent regimes, which is particularly important in applications where structural variability is partially explained by external factors. When X_i is the 1-column, i.e., the intercept, the MoE model reduces to the mixture model.

The identifiability of the MoE-Wishart model follows from general results for mixtures of exponential family experts [10]. Specifically, the model is identifiable up to a permutation of the latent cluster labels, provided the cluster-specific Wishart distributions are distinct and the covariate design matrix is of full rank. The constraint $\beta_K \equiv 0$ resolves the translational non-identifiability inherent to the multinomial logistic gating network, ensuring unique parameter estimation for a given labeling of the mixture components.

3 Bayesian approaches and MCMC algorithms

In this section, we introduce a Bayesian framework together with MCMC sampling algorithms specifically designed for the mixture and MoE-Wishart models. To the best of our knowledge, this constitutes a novel contribution.

3.1 Bayesian mixture-Wishart model

We place the following priors distribution on the parameters in the mixture model in (3):

$$z_i \mid \boldsymbol{\pi} \sim \text{Categorical}(\pi_1, \dots, \pi_K), \\ \boldsymbol{\pi} \sim \text{Dirichlet}(\alpha_1, \dots, \alpha_K), \\ \Sigma_k \sim \mathcal{IW}(\nu_0, \Psi_0^{-1}), \quad k = 1, \dots, K,$$

where $\mathcal{IW}(\nu_0, \Psi_0^{-1})$ denotes the inverse-Wishart prior on Σ_k with degrees of freedom ν_0 and scale matrix Ψ_0^{-1} (we follow the common conjugate parametrization where the posterior for Σ_k is inverse-Wishart with updated parameters). For the cluster Wishart degrees ν_k we place an independent Gamma prior:

$$p(\nu_k) \propto \nu_k^{a-1} e^{-b\nu_k}, \quad \nu_k > 0,$$

with hyper-parameters $a > 0, b > 0$. In practice the sampler enforces $\nu_k > p - 1$. The Dirichlet hyperparameters $(\alpha_1, \dots, \alpha_K)$ control prior concentration of the mixture weights, we use a symmetric specification $\alpha_k = \alpha_0/K$ by default, where smaller α_0 favors sparse component usage and larger α_0 favors near-uniform weights. For the inverse-Wishart prior, ν_0 determines prior strength and is set to $\nu_0 = p + 2$ for a weakly informative prior with finite mean, while Ψ_0 is chosen proportional to the identity matrix. The Gamma hyperparameters (a, b) for ν_k are selected so the prior mean a/b lies moderately above $p - 1$, ensuring validity while remaining weakly informative.

Let $\Theta = \{\boldsymbol{\pi}, z_{1:n}, (\nu_k, \Sigma_k)_{k=1}^K\}$. The joint posterior distribution is

$$p(\Theta | S_{1:n}) \propto \left[\prod_{i=1}^n \prod_{k=1}^K \{\pi_k f_{\mathcal{W}}(S_i | \nu_k, \Sigma_k)\}^{1_{\{z_i=k\}}} \right] p(\boldsymbol{\pi}) \prod_{k=1}^K p(\Sigma_k) p(\nu_k).$$

Conditioning on the latent labels yields a factorized posterior structure that enables efficient Gibbs sampling with a Metropolis–Hastings step for ν_k .

Below we give each update used in the Gibbs sampler and the Metropolis–Hastings (MH) step for ν_k . The entire procedure is summarized in Algorithm 1.

Step 1: Conditional of the labels z_i .

The posterior probability that $z_i = k$ (up to normalization) is

$$p(z_i = k | S_i, \{\Sigma_\ell, \nu_\ell\}, \boldsymbol{\pi}) \propto \pi_k f_{\mathcal{W}}(S_i | \nu_k, \Sigma_k). \quad (6)$$

Hence compute the log-unnormalized weights

$$\ell_{ik} = \log \pi_k + \frac{\nu_k - p - 1}{2} \log |S_i| - \frac{1}{2} \text{tr}(\Sigma_k^{-1} S_i) - \frac{\nu_k p}{2} \log 2 - \frac{\nu_k}{2} \log |\Sigma_k| - \log \Gamma_p\left(\frac{\nu_k}{2}\right), \quad (7)$$

and sample z_i from categorical probabilities proportional to ℓ_{ik} , using $\exp(\ell_{ik} - \max_k \ell_{ik})$ instead for numerical stability. These ℓ_{ik} are used both to sample labels and to compute the observed-data log-likelihood for monitoring. Note that by integrating out $\boldsymbol{\pi}$ we have $p(z_i = k | S_i, \{\Sigma_\ell, \nu_\ell\}, \boldsymbol{\pi}) \propto f_{\mathcal{W}}(S_i | \nu_k, \Sigma_k) \cdot (\alpha_k + n_{-i,k})$, see Appendix A for details, which may make Gibbs sampling mixing better.

Step 2: Conditional of the weights $\boldsymbol{\pi}$.

Given counts n_k the posterior for $\boldsymbol{\pi}$ is Dirichlet distributed:

$$\boldsymbol{\pi} | \mathbf{z} \sim \text{Dirichlet}(\alpha_1 + n_1, \dots, \alpha_K + n_K).$$

Step 3: Conditional of the cluster scale matrices Σ_k .

Given assignments $\{z_i\}$ and the cluster degrees ν_k , the prior $\Sigma_k \sim \mathcal{IW}(\nu_0, \Psi_0^{-1})$ is conjugate with the Wishart likelihood. The posterior is an inverse-Wishart:

$$\Sigma_k | \{S_i : z_i = k\}, \nu_k \sim \mathcal{IW}\left(\nu_0 + n_k \nu_k, \Psi_0^{-1} + S_{(k)}\right),$$

i.e. degrees $\nu_0 + n_k \nu_k$ and scale matrix $\Psi_0^{-1} + S_{(k)}$, where $S_{(k)} = \sum_{i \in I_k} S_i$ and $I_k = \{i : z_i = k\}$. Note: when $n_k = 0$ (i.e., the cluster k diminishes) we sample Σ_k from the prior $\mathcal{IW}(\nu_0, \Psi_0^{-1})$.

Step 4: Update of ν_k (MH on log scale).

The degrees of freedom ν_k do not admit a convenient conjugate update; we update each ν_k using a MH step proposing on the log scale. Let the current value be ν and propose

$$\log \nu^* \sim \mathcal{N}(\log \nu, \sigma_{\text{MH}}^2), \quad \nu^* = \exp(\log \nu^*).$$

The log posterior for ν (for cluster k)—using the cluster-specific summarized quantities n_k , $S_{(k)}$, and $L_{(k)} = \sum_{i \in I_k} \log |S_i|$ —is, up to an additive constant,

$$\begin{aligned} & \log p(\nu \mid \{S_i\}_{i \in I_k}, \Sigma_k) \\ &= \sum_{i \in I_k} \log f_{\mathcal{W}}(S_i \mid \nu, \Sigma_k) + \log p(\nu) \\ &= \frac{\nu - p - 1}{2} L_{(k)} - \frac{1}{2} \text{tr}(\Sigma_k^{-1} S_{(k)}) - n_k \left(\frac{\nu p}{2} \log 2 + \frac{\nu}{2} \log |\Sigma_k| + \log \Gamma_p\left(\frac{\nu}{2}\right) \right) \\ & \quad + (a - 1) \log \nu - \nu b. \end{aligned}$$

If we denote by $\ell(\nu)$ the log-posterior, then the acceptance probability for the proposal ν^* is

$$\alpha = \min \{1, \exp(\ell(\nu^*) + \log \nu^* - \ell(\nu) - \log \nu)\},$$

where the extra $\log \nu$ terms are the Jacobian corrections. We only attempt the MH update for proposals with $\nu^* > p - 1$.

Algorithm 1 Gibbs sampler for Wishart mixture with ν_k via MH

- 1: **Inputs:** S_1, \dots, S_n , number of clusters K , hyperparameters α, ν_0, Ψ_0 , MH proposal scale σ_{MH} , iterations N , burn-in, thin.
- 2: **Initialize:** Vectorize S_i to form S_{mat} (size $n \times p^2$); compute $\log |S_i|$ for all i . Initialize labels z_i (k-means on $\text{vec}(S_i)$ suggested), $\pi_k = n_k/n$, ν_k (e.g., $p + 2$), and Σ_k (cluster sample / prior).
- 3: **for** $\text{iter} = 1, \dots, N$ **do**
- 4: ▷ **Step 1 (labels):** For each cluster k compute Σ_k^{-1} , $\log |\Sigma_k|$ and $\text{tr}(\Sigma_k^{-1} S_i)$, and draw labels from

$$p(z_i = k \mid S_i, \{\Sigma_\ell, \nu_\ell\}, \boldsymbol{\pi}) \propto f_{\mathcal{W}}(S_i \mid \nu_k, \Sigma_k) \cdot (\alpha_k + n_{-i,k})$$

- 5: ▷ **Step 2 (weights):** Set $n_k = \#\{i : z_i = k\}$ and draw

$$\boldsymbol{\pi} \sim \text{Dirichlet}(\alpha_1 + n_1, \dots, \alpha_K + n_K).$$

- 6: ▷ **Step 3 (scale matrices):** For each k , compute $S_{(k)}$ and draw

$$\Sigma_k \sim \mathcal{IW}(\nu_0 + n_k \nu_k, \Psi_0^{-1} + S_{(k)}).$$

If $n_k = 0$ draw from prior $\mathcal{IW}(\nu_0, \Psi_0^{-1})$.

- 7: ▷ **Step 4 (degrees ν_k):**
- 8: For each k , propose $\log \nu^* \sim \mathcal{N}(\log \nu_k, \sigma_{\text{MH}}^2)$ and accept with probability

$$\min \{1, \exp(\ell(\nu^*) + \log \nu^* - \ell(\nu_k) - \log \nu_k)\},$$

where $\ell(\nu)$ is the log posterior for cluster k computed using $n_k, L_{(k)}, S_{(k)}$ and Σ_k .

- 9: ▷ **Record / monitor:** Compute log-likelihood; save samples.

10: **end for**

11: **Return:** posterior draws of $\boldsymbol{\pi}, \{\nu_k\}, \{\Sigma_k\}, \{z_i\}$ and monitoring diagnostics.

Practical implementation: Computation of the trace terms is further optimized via the vectorization identity $\text{tr}(AB) = \text{vec}(A)^\top \text{vec}(B)$, enabling simultaneous evaluation of $\text{tr}(\Sigma_k^{-1} S_i)$ across all i through the product of an $n \times p^2$ matrix, formed by rows of $\text{vec}(S_i)^\top$, and the vector $\text{vec}(\Sigma_k^{-1})$. Numerical precision is maintained by employing Cholesky decompositions for matrix inversions and determinant calculations—incorporating a minimal diagonal jitter (e.g., $10^{-6} I_p$) to condition ill-behaved matrices—and utilizing Bartlett decompositions for stable inverse-Wishart sampling. Finally, the algorithm adopts

weakly informative priors (e.g., $\nu_0 = p + 2$, $\Psi_0 = I_p$) and employs log-space MH proposals with scales σ_{MH}^2 (can be cluster-specific) tuned to acceptance rates of 20–40%, utilizing log-sum-exp operations to ensure precision in density calculations.

3.2 Bayesian MoE–Wishart model

We put the following prior distributions on the parameters for the MoE–Wishart model in (5):

$$\Sigma_k \sim \mathcal{IW}(\nu_0, \Psi_0), \quad \nu_k \sim \text{Gamma}(a_\nu, b_\nu), \quad \beta_{1:(K-1)} \stackrel{\text{iid for columns}}{\sim} \mathcal{N}_q(0, \sigma_\beta^2 I_q).$$

Let $\Theta = \{z_{1:n}, (\nu_k, \Sigma_k)_{k=1}^K, \beta_{1:(K-1)}\}$. The joint posterior is

$$p(\Theta \mid S_{1:n}, X_{1:n}) \propto \prod_{i=1}^n \prod_{k=1}^K \left[\pi_{ik}(X_i; \beta), f_{\mathcal{W}}(S_i \mid \nu_k, \Sigma_k) \right]^{\mathbf{1}_{\{z_i=k\}}} \prod_{k=1}^K p(\Sigma_k) p(\nu_k) \prod_{k=1}^{K-1} p(\beta_k).$$

Conditioning on the latent labels yields a factorized posterior structure that enables efficient Gibbs sampling with a MH step for ν_k .

The entire Metropolis-within-Gibbs sampling for the MoE–Wishart model is as follows.

Step 1: Update labels z_i (categorical sampling).

The posterior probability of $z_i = k$ is

$$\Pr(z_i = k \mid S_i, X_i, \Theta) = \frac{\exp(\ell_{ik})}{\sum_{\ell=1}^K \exp(\ell_{i\ell})},$$

where Θ collects all coefficients $\beta_1, \dots, \beta_{K-1}$, and z_i is sampled from this categorical distribution, with ℓ_{ik} given in (7).

Step 2: Update gating coefficients $\beta_{1:(K-1)}$ (Metropolis–Hastings).

We use MH sampling to update the coefficients in blocks by cluster. Specifically, for each $k = 1, \dots, K-1$, we propose

$$\beta_k^* = \beta_k + \varepsilon_k, \quad \varepsilon_k \sim \mathcal{N}(0, \sigma_{\beta_k}^2 I),$$

while fixing $\beta_K \equiv 0$ for identifiability. Let π_{ik}^* denote the gating probabilities computed under the proposed coefficients β^* . Under a zero-mean Gaussian prior with variance σ_β^2 , the log prior difference is $\Delta \log p(\beta) = -\frac{1}{2\sigma_\beta^2} \sum_{k=1}^{K-1} (\|\beta_k^*\|_2^2 - \|\beta_k\|_2^2)$. Conditioned on the latent cluster labels z , the gating likelihood is $\log p(\mathbf{z} \mid X, \beta) = \sum_{i=1}^n \log \pi_{i,z_i}$. The MH log target ratio is therefore

$$\log \alpha = \sum_{i=1}^n (\log \pi_{i,z_i}^* - \log \pi_{i,z_i}) + \Delta \log p(\beta).$$

The proposal is accepted with probability $\min\{1, \exp(\log \alpha)\}$.

Step 3: Update Σ_k (conjugate inverse–Wishart).

Each Σ_k is updated sequentially from its inverse–Wishart posterior:

$$\Sigma_k \mid \text{rest} \sim \mathcal{IW}\left(\nu_0 + n_k \nu_k, \Psi_0^{-1} + S_{(k)}\right),$$

where $n_k = |I_k|$, $I_k = \{i : z_i = k\}$, and $S_{(k)} = \sum_{i \in I_k} S_i$.

Step 4: Update degrees of freedom ν_k (MH on log scale).

Each ν_k is updated sequentially via a log-normal random-walk proposal:

$$\log \nu_k^* \sim \mathcal{N}(\log \nu_k, \sigma_\nu^2), \quad \nu_k^* = \exp(\log \nu_k^*).$$

Using summarized quantities $S_{(k)}$ and $L_{(k)} = \sum_{i \in I_k} \log |S_i|$, the log joint density (data + prior) that depends on ν is

$$\ell(\nu) = \sum_{i \in I_k} \left\{ \frac{\nu - p - 1}{2} \log |S_i| - \frac{\nu p}{2} \log 2 - \frac{\nu}{2} \log |\Sigma_k| - \log \Gamma_p\left(\frac{\nu}{2}\right) \right\} \\ + (a_\nu - 1) \log \nu - \nu b_\nu + C,$$

where C collects terms not depending on ν . Using $L_{(k)}$ and $\text{tr}(\Sigma_k^{-1} S_{(k)})$ we compute differences efficiently. The MH log target ratio is

$$\log \alpha = [\ell(\nu^*) + \log \nu^*] - [\ell(\nu) + \log \nu],$$

where the extra $\log \nu$ terms are the change-of-variable Jacobian from the log proposal. Accept ν^* with probability $\min(1, \exp(\log \alpha))$.

3.3 Selection of K

Let K denote the number of experts in the mixture-of-experts (MoE) model defined in (5). Because increasing K always weakly improves the in-sample likelihood, model selection must trade off goodness of fit against model complexity. We therefore select K using information criteria and Bayesian predictive measures that are appropriate for latent-mixture models.

3.3.1 Model dimension

Let p be the dimension of the Wishart random matrix S_i and let q denote the dimension of the covariate vector X_i (including an intercept). Each expert k contributes a Wishart scale matrix $\Sigma_k \in \mathbb{S}_+^p$ with $\frac{p(p+1)}{2}$ free parameters and a degrees-of-freedom parameter $\nu_k > p - 1$. Hence, each expert contributes $\frac{p(p+1)}{2} + 1$ free parameters. The softmax gating network is identifiable only up to a baseline; setting $\beta_K = 0$ yields $(K - 1)q$ free gating parameters. The total dimension of the model is therefore

$$\mathcal{D}_K = K \left(\frac{p(p+1)}{2} + 1 \right) + (K - 1)q.$$

3.3.2 Bayesian Information Criterion

Let $\hat{\Theta}_K$ denote the maximum likelihood or posterior mode estimator under a K -component model. The Bayesian Information Criterion (BIC) is defined as

$$\text{BIC}(K) = -2\ell(\hat{\Theta}_K) + \mathcal{D}_K \log n,$$

where $\ell(\Theta)$ is the observed-data log-likelihood in (8).

3.3.3 Integrated Completed Likelihood

Because mixture models may artificially increase K by splitting existing components, we also consider the Integrated Completed Likelihood (ICL) [2], which penalizes posterior uncertainty in class assignments. Let $r_{ik} = \Pr(z_i = k \mid S_i, X_i, \hat{\Theta}_K)$ denote the posterior responsibilities. The ICL criterion is

$$\text{ICL}(K) = \text{BIC}(K) - 2 \sum_{i=1}^n \sum_{k=1}^K r_{ik} \log r_{ik}.$$

The entropy term favors models with well-separated experts and thus selects the number of substantively distinct regimes.

3.3.4 Bayesian LOO

To compare Bayesian predictive models, out-of-sample pointwise predictive accuracy can be estimated using leave-one-out cross-validation (LOO) or the widely applicable information criterion (WAIC). Both approaches are based on evaluating the log-likelihood at posterior draws, and WAIC is asymptotically equivalent to LOO. However, [33] show that LOO implemented via Pareto-smoothed importance sampling (PSIS) is more robust in finite samples, particularly in the presence of weak priors or influential observations.

The expected log pointwise predictive density (elpd) under LOO is defined as

$$\text{elpd}_{\text{loo}} = \sum_{i=1}^n \log p(S_i | S_{-i}), \quad p(S_i | S_{-i}) \approx \left(\frac{1}{N} \sum_{t=1}^N \frac{1}{p(S_i | \Theta^{(t)})} \right)^{-1}.$$

where S_{-i} denotes the data with the i -th observation removed, and $p(S_i | S_{-i})$ can be approximately estimated by the importance sampling using posterior draws $\{\Theta^{(t)}\}_{t=1}^N$ from $p(\Theta | S)$, where $\Theta^{(t)}$ denotes the full parameter vector at the t -th MCMC iteration. Because the raw importance ratios can be heavy-tailed, PSIS replaces their upper tail with a fitted generalized Pareto distribution, yielding stabilized importance weights and a diagnostic shape parameter that indicates the reliability of the approximation. The resulting LOO estimator of predictive accuracy is

$$\widehat{\text{elpd}}_{\text{loo}} = \sum_{i=1}^n \widehat{\text{elpd}}_{\text{loo},i} = \sum_{i=1}^n \log p(S_i | S_{-i}),$$

where $\widehat{\text{elpd}}_{\text{loo},i}$ denotes the contribution of observation i .

3.3.5 Model selection rule

We select the number of experts K by combining these complementary criteria. BIC provides consistency for large samples, ICL identifies the number of economically meaningful regimes, and elpd_{loo} is particularly useful for assessing the predictive performance of Bayesian methods. In practice, we choose the smallest K that minimizes BIC and ICL, or maximizes elpd_{loo} for Bayesian methods.

4 Maximum likelihood and EM algorithm

4.1 Maximum likelihood estimation

The inference of classical Wishart mixture models was carried out via the Expectation–Maximization (EM) algorithm in [8]. Here we estimate the parameters of the mixture-of-experts (MoE) model in (5) by maximum likelihood using the EM algorithm. The EM framework is particularly well suited here because the likelihood involves a latent mixture structure induced by the unobserved component labels.

Let $\Theta = \{(\beta_k, \nu_k, \Sigma_k)_{k=1}^K\}$ denote the model parameters under the MoE formulation. The observed-data log-likelihood of the MoE model (5) is:

$$\ell(\Theta) = \sum_{i=1}^n \log \left(\sum_{k=1}^K \pi_{ik}(X_i; \beta) \cdot f_{\mathcal{W}}(S_i | \nu_k, \Sigma_k) \right). \quad (8)$$

Because of the summation inside the logarithm, direct maximization is analytically intractable. The EM algorithm overcomes this difficulty by introducing the latent class labels z_i and iteratively maximizing a tractable surrogate objective.

If the latent cluster labels z_i were observed, the complete-data log-likelihood (up to additive constants) would be:

$$\ell_c(\Theta) = \sum_{i=1}^n \sum_{k=1}^K z_{ik} \left[\log \pi_{ik}(X_i; \beta) + \log f_{\mathcal{W}}(S_i | \nu_k, \Sigma_k) \right],$$

which, after inserting the Wishart density, becomes:

$$\begin{aligned} \ell_c(\Theta) = \sum_{i=1}^n \sum_{k=1}^K z_{ik} & \left[\frac{\nu_k - p - 1}{2} \log |S_i| - \frac{\nu_k}{2} \log |\Sigma_k| - \frac{1}{2} \text{tr}(\Sigma_k^{-1} S_i) \right. \\ & \left. - \log \Gamma_p \left(\frac{\nu_k}{2} \right) - \frac{\nu_k p}{2} \log 2 + \log \pi_{ik}(X_i; \beta) \right]. \quad (9) \end{aligned}$$

This representation reveals that the gating parameters β and the expert parameters (ν_k, Σ_k) enter the likelihood in separable blocks, which yields convenient conditional maximization steps.

4.2 EM algorithm

Let $z_i \in \{1, \dots, K\}$ denote the latent cluster labels of observation i , and define the posterior responsibility:

$$r_{ik} := \Pr(z_i = k | S_i, X_i, \Theta).$$

We introduce some summarized quantities to simplify notation:

$$n_k = \sum_{i=1}^n r_{ik}, \quad M_k = \sum_{i=1}^n r_{ik} S_i, \quad \overline{\log |S|}_k = \frac{1}{n_k} \sum_{i=1}^n r_{ik} \log |S_i|, \quad \overline{S}_k = \frac{M_k}{n_k}.$$

The EM algorithm alternates between computing “soft” assignments (responsibilities) of observations to experts via the gating network (E-step) and updating the gating coefficients β via weighted multinomial logistic regression and the expert parameters (ν_k, Σ_k) via weighted maximum likelihood (M-step). This alternating optimization usually yields a monotone non-decreasing observed-data log-likelihood at every iteration, and provides a stable, statistically principled estimator for the MoE–Wishart model.

E-step. At iteration (t) , we compute the posterior responsibilities:

$$r_{ik}^{(t)} = \Pr(z_i = k | S_i, X_i, \Theta^{(t)}) = \frac{\pi_{ik}(X_i; \beta^{(t)}) f_{\mathcal{W}}(S_i | \nu_k^{(t)}, \Sigma_k^{(t)})}{\sum_{j=1}^K \pi_{ij}(X_i; \beta^{(t)}) f_{\mathcal{W}}(S_i | \nu_j^{(t)}, \Sigma_j^{(t)})}.$$

These weights quantify the probability that observation i originates from expert k , given the current parameter estimates.

M-step. Maximizing the conditional expectation of the complete-data log-likelihood:

$$Q(\Theta | \Theta^{(t)}) = \sum_{i=1}^n \sum_{k=1}^K r_{ik}^{(t)} \left[\log \pi_{ik}(X_i; \beta) + \log f_{\mathcal{W}}(S_i | \nu, \Sigma) \right].$$

• First, update of gating network (β) : The update for β corresponds to a weighted multinomial logistic regression:

$$\beta^{(t+1)} = \arg \max_{\beta} \sum_{i=1}^n \sum_{k=1}^K r_{ik}^{(t)} \log \pi_{ik}(X_i; \beta).$$

This optimization problem has no closed-form solution and is solved numerically, for example via BFGS or Newton–Raphson method.

- Second, update of scale matrices (Σ_k): For fixed ν_k , the maximizer of $Q(\Theta \mid \Theta^{(t)})$ with respect to Σ_k admits a closed-form expression:

$$\Sigma_k^{(t+1)} = \frac{1}{n_k \nu_k^{(t+1)}} \sum_{i=1}^n r_{ik}^{(t)} S_i = \frac{\bar{S}_k}{\nu_k^{(t+1)}}.$$

- Third, update of degrees of freedom (ν_k): The update for ν_k is obtained by solving the score equation:

$$\psi_p\left(\frac{\nu_k}{2}\right) - \log \nu_k + \log\left(\frac{|M_k|}{n_k}\right) - \log |\bar{S}_k| + p \log 2 - p \log n_k = 0,$$

where $\psi_p(\cdot)$ denotes the multivariate digamma function. This nonlinear equation is solved numerically using Newton–Raphson or a similar root-finding method.

5 Simulations studies

The code to reproduce the simulation results is available at https://github.com/zhizhui/moewishart/tree/main/numerical_studies.

5.1 Simulation with mixture model

5.1.1 Setup

We consider a finite mixture of Wishart distributions with $K = 3$ clusters. The mixture weights are fixed at $\pi = (\pi_1, \pi_2, \pi_3) = (0.35, 0.40, 0.25)$. We vary sample sizes $n \in \{200, 500, 1000\}$ and matrix dimensions $p \in \{2, 8\}$. Each positive definite observed covariance matrix S_i , $i = 1, \dots, n$, is generated independently from the mixture model

$$S_i \sim \sum_{k=1}^3 \pi_k \mathcal{W}_p(\nu_k, \Sigma_k),$$

where $\mathcal{W}_p(\nu_k, \Sigma_k)$ denotes the p -dimensional Wishart distribution with degrees of freedom ν_k and scale matrix Σ_k . The degrees of freedom are specified with two cases corresponding to the two options of the matrix dimension p :

$$(\nu_1, \nu_2, \nu_3) = \begin{cases} (8, 12, 3), & \text{if } p = 2, \\ (9, 20, 14), & \text{if } p = 8. \end{cases}$$

Similarly the scale matrices Σ_k 's are specified with cases corresponding to the matrix dimensions:

- If $p = 2$, we set $\Sigma_1 = \begin{pmatrix} 0.5 & 0.2 \\ 0.2 & 0.7 \end{pmatrix}$, $\Sigma_2 = \begin{pmatrix} 2.0 & 0.6 \\ 0.6 & 1.5 \end{pmatrix}$, $\Sigma_3 = \begin{pmatrix} 4.0 & 0.2 \\ 0.2 & 3.0 \end{pmatrix}$.
- If $p = 8$, we take $\Sigma_1 = \{0.5^{|j-j'|}\}_{jj'}$, $\Sigma_2 = \{0.2^{|j-j'|}\}_{jj'}$, $\Sigma_3 = \{0.8^{|j-j'|}\}_{jj'}$, $j, j' \in \{1, \dots, p\}$.

Considered methods: For each simulation setup, we evaluate four competing estimation approaches:

- Two are based on finite mixture models: the full Bayesian method (denoted by **Bayes**) and the maximum likelihood estimator implemented via the EM algorithm (denoted by **EM**).
- The other two approaches are based on the mixture-of-experts framework: the full Bayesian approach (denoted by **Bayes-MoE**) and the EM-based maximum likelihood (denoted by **EM-MoE**). More specifically, only intercepts are included for both **Bayes-MoE** and **EM-MoE** as concomitant covariates and the gating probabilities π_{ik} are reduced to π_k .

For the two full Bayesian versions (i.e., **Bayes** and **Bayes-MoE**), we run MCMC with 20000 iterations, of which the first 5000 iterations are discarded as the burn-in period.

Model performance evaluation: we use the average over all components errors to access the performance of the considered methods. More specifically, we consider the following metrics:

$$\frac{1}{K} \|\hat{\boldsymbol{\pi}} - \boldsymbol{\pi}\|_1; \quad \frac{1}{K} \|\hat{\boldsymbol{\nu}} - \boldsymbol{\nu}\|_1; \quad \frac{1}{K} \sum_{k=1}^K \|\hat{\boldsymbol{\Sigma}}_k - \boldsymbol{\Sigma}_k\|_2^2.$$

For the two full Bayesian versions (i.e., **Bayes** and **Bayes-MoE**), posterior mean estimators are used to calculate the evaluation metrics. We generate 100 data sets for each simulation setting and report the results in Figure 1.

5.1.2 Simulations results

Figure 1 illustrates that the estimation accuracy of all four methods—**Bayes**, **EM**, **Bayes-MoE**, and **EM-MoE**—for the parameters $\boldsymbol{\nu}$, $\boldsymbol{\Sigma}_k$, and $\boldsymbol{\pi}$ improves systematically with increasing sample size under data generated from the mixture model.

For $p = 2$, Figure 1A shows that the correctly specified mixture-model **EM** approach yields larger estimation errors than the other three approaches at the smallest sample size ($n = 200$) and large outliers at sample sizes $n \in \{500, 1000\}$. These outliers arise because the estimates $\boldsymbol{\nu}$, $\boldsymbol{\Sigma}_{1:K}$ and $\boldsymbol{\pi}$ obtained by **EM** failed to converge for those simulated data sets. The correctly specified mixture-model **Bayes** and mixture-of-experts methods (**Bayes-MoE** and **EM-MoE**) achieve similar estimation errors for $\boldsymbol{\nu}$, $\boldsymbol{\Sigma}_{1:K}$, and $\boldsymbol{\pi}$ across all sample sizes considered ($n \in 200, 500, 1000$). Figure 1B for $p = 8$ indicates that all four approaches have comparable performance, except that the **EM** approach consistently produces a few outliers due to convergence issues of $\boldsymbol{\nu}$, $\boldsymbol{\Sigma}_{1:K}$ and $\boldsymbol{\pi}$ for some simulated data sets.

Supplementary Figures S7 ($p = 2$) and S8 ($p = 8$) demonstrate stable Markov chain Monte Carlo (MCMC) behavior for the Bayesian methods (**Bayes** and **Bayes-MoE**), as evidenced by the log-likelihood trace plots for each working model. In addition, cluster-specific parameters— π_k , ν_k , and $\log |\boldsymbol{\Sigma}_k|$ for **Bayes**, and ν_k and $\log |\boldsymbol{\Sigma}_k|$ for **Bayes-MoE** ($k \in 1, 2, 3$)—exhibit satisfactory mixing. As expected, larger fluctuations in the trace plots are observed for $n = 200$ relative to $n = 500$ and $n = 1000$. Table 1 reports effective sample sizes (ESS) for selected parameters, showing systematically smaller ESS values with larger variations at $n = 200$ compared to larger sample sizes for both Bayesian approaches. Finally, Supplementary Figures S11A–B confirm that the EM algorithms, for both the mixture and MoE working models, converge reliably in terms of the log-likelihood across all simulation scenarios based on one simulated data set.

5.2 Simulation with mixture-of-experts model

5.2.1 Setup

We extend the finite mixture of Wishart distributions to a mixture-of-experts setting with covariate-dependent mixing proportions. As before, we take $K = 3$ latent clusters, and examine sample sizes $n \in \{200, 500, 1000\}$ and matrix dimensions $p \in \{2, 8\}$.

With $q = 3$, let $X \in \mathbb{R}^{n \times q}$ denote the covariate matrix where the entries are independently generated as $x_{ij} \sim \mathcal{N}(0, 1)$. The mixing proportions are obtained via a multinomial logistic (softmax) function

$$\pi_{ik}(X_i; \beta) = \frac{\exp\{X_i^\top \beta_k\}}{\sum_{l=1}^K \exp\{X_i^\top \beta_l\}}, \quad i = 1, \dots, n, \quad k = 1, \dots, K,$$

with covariate effects $\beta_{1:K} \in \mathbb{R}^{q \times K}$ and the reference constraint $\beta_K = \mathbf{0}$ for identifiability. Each coordinate of the effect β is independently simulated from a uniform distribution, $\beta_{jk} \sim \mathcal{U}(-2, 2)$, and $\beta_{1:K}$ is the same for every simulation.

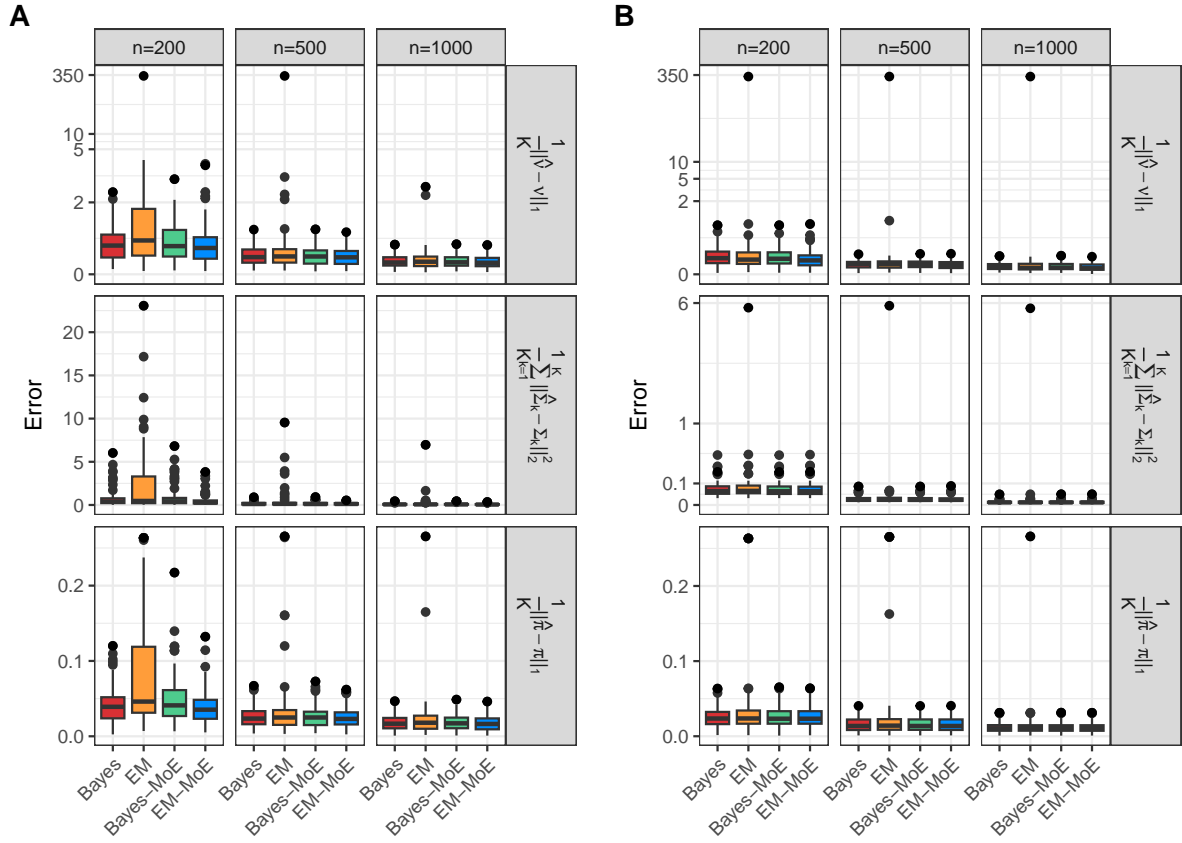


Figure 1: Simulation results. Data were generated from finite mixture models over 100 Monte Carlo replications. Results are reported for sample sizes $n \in \{200, 500, 1000\}$ under two dimensional settings: (A) $p = 2$ and (B) $p = 8$. The four competing methods compared include: (i) Bayesian mixture models (**Bayes**); (ii) EM-based mixture models (**EM**); (iii) Bayesian mixture-of-experts models (**Bayes-MoE**); and (iv) EM-based mixture-of-experts models (**EM-MoE**). Estimation performance is evaluated using average componentwise errors: $\frac{1}{K} \|\hat{\pi} - \pi\|_1$; $\frac{1}{K} \|\hat{\nu} - \nu\|_1$; $\frac{1}{K} \sum_{k=1}^K \|\hat{\Sigma}_k - \Sigma_k\|_2^2$.

Table 1: Effective sample sizes (ESS) from MCMC for Bayes and Bayes-MoE methods. Data is generated from the mixture model. Reported are the mean and standard deviation of ESS over 100 simulations for selected parameters.

Working model	ν		Σ		π	
	ν_1	ν_2	$\Sigma_{1,11}$	$\Sigma_{2,11}$	π_1	π_2
Mixture model: $p = 2$						
$n = 200$	675 (250)	164 (64)	1079 (525)	214 (88)	395 (244)	907 (865)
$n = 500$	825 (140)	204 (43)	1339 (349)	259 (61)	500 (155)	1040 (455)
$n = 1000$	794 (110)	183 (31)	1192 (298)	222 (45)	433 (107)	894 (331)
Mixture model: $p = 8$						
$n = 200$	1295 (91)	760 (69)	8528 (797)	3303 (514)	14651 (481)	14641 (541)
$n = 500$	1413 (85)	838 (47)	8907 (604)	3709 (338)	14922 (323)	14965 (263)
$n = 1000$	1340 (87)	829 (56)	9179 (651)	3559 (324)	14990 (100)	14992 (99)
MoE model: $p = 2$						
$n = 200$	622 (266)	170 (70)	1029 (521)	228 (227)	-	-
$n = 500$	713 (158)	179 (36)	1085 (322)	213 (47)	-	-
$n = 1000$	678 (138)	176 (33)	999 (267)	199 (44)	-	-
MoE model: $p = 8$						
$n = 200$	1315 (91)	814 (66)	8784 (871)	3597 (462)	-	-
$n = 500$	1387 (73)	851 (49)	9069 (570)	3610 (301)	-	-
$n = 1000$	1349 (54)	821 (47)	8837 (607)	3565 (316)	-	-

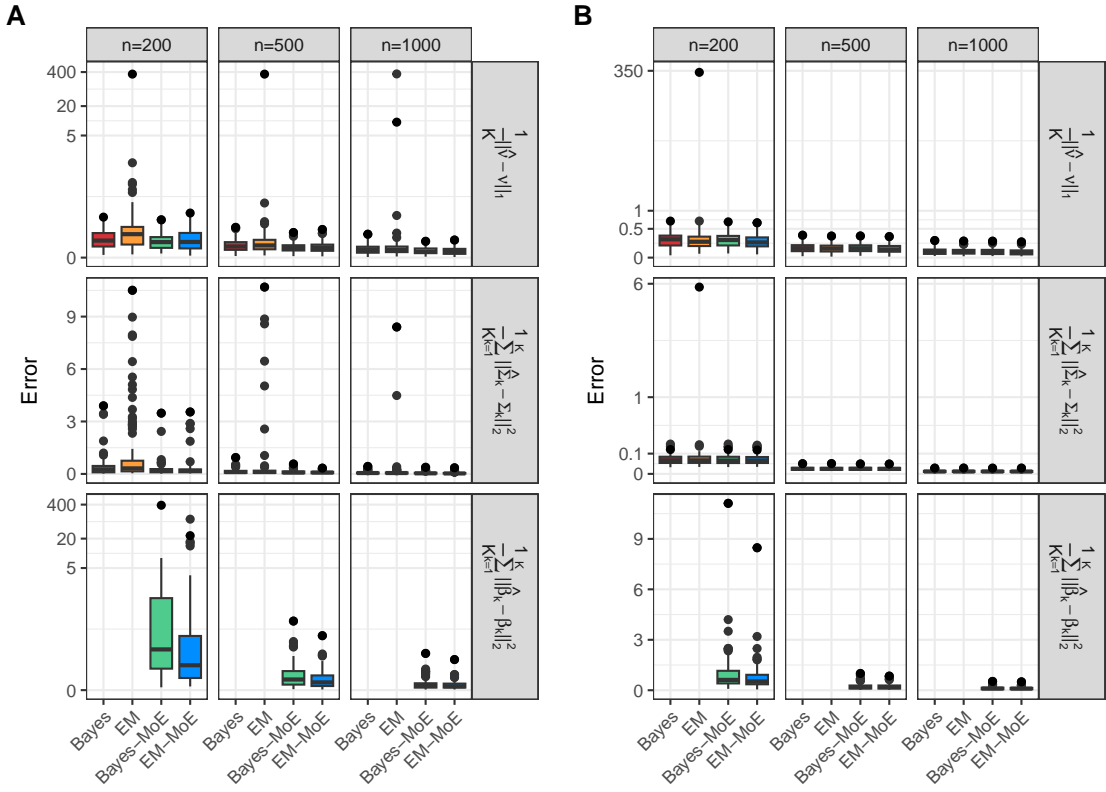


Figure 2: Simulation results. Data were generated from the **mixture-of-experts (MoE) model** across 100 simulated data sets. Panels (A) and (B) correspond to the settings $p = 2$ and $p = 8$, respectively. The four competing methods compared are: (i) Bayesian inference under the mixture model (**Bayes**); (ii) EM-based inference under the mixture model (**EM**); (iii) Bayesian inference under the mixture-of-experts model (**Bayes-MoE**); and (iv) EM-based inference under the mixture-of-experts model (**EM-MoE**).

Conditional on X_i , each positive definite matrix S_i is independently generated from the mixture-of-experts model

$$S_i \sim \sum_{k=1}^3 \pi_{ik}(X^\top \beta) \mathcal{W}_p(\nu_k, \Sigma_k), \quad i = 1, \dots, n$$

Here the cluster parameters (ν_k, Σ_k) are the same as in the finite mixture setup in Section 5.1.1.

Model performance evaluation: we use the average over all cluster errors to access the performance of the considered methods. More specifically, we consider the following metrics:

$$\frac{1}{K} \|\hat{\nu} - \nu\|_1; \quad \frac{1}{K} \sum_{k=1}^K \|\hat{\Sigma}_k - \Sigma_k\|_2^2; \quad \frac{1}{K} \sum_{k=1}^K \|\hat{\beta}_k - \beta_k\|_2^2.$$

All other setups remain the same as the finite mixture case in Section 5.1.1.

5.2.2 Simulations results

As in the mixture-model setting, Figure 2 demonstrates that estimation accuracy under the mixture-of-experts model improves monotonically with increasing sample size (Figure 2A for $p = 2$ and Figure 2B for $p = 8$). **Bayes-MoE** and **EM-MoE** exhibit comparable performance across all scenarios. At the smallest sample size ($n = 200$) for both $p = 2$ and $p = 8$, **Bayes-MoE** yields slightly smaller estimation error for ν than **EM-MoE**, while incurring marginally larger error for β (bottom-left panels). The mixture-model-based methods (**Bayes** and **EM**) perform slightly worse than the correctly specified MoE-based approaches, with **EM** consistently producing the largest estimation errors across metrics for $p = 2$. For $p = 8$, **EM** also consistently produces a few outliers due to convergence issues of ν and $\Sigma_{1:K}$ for some simulated data sets.

For data generated from the MoE model, Supplementary Figures S9 ($p = 2$) and S10 ($p = 8$) further indicate stable Markov chain Monte Carlo (MCMC) behavior for both Bayesian methods, as evidenced by log-likelihood trace plots and component-specific parameter trajectories for each working model. Consistent with the mixture-model results, larger fluctuations are observed at $n = 200$ relative to $n = 500$ and $n = 1000$. Table S3 reports effective sample sizes (ESS) for selected parameters, which increase systematically with sample size for both Bayesian approaches. Finally, Supplementary Figure S11C-D confirms convergence of the EM algorithms in terms of the log-likelihood for both the mixture and mixture-of-experts working models across both scenarios $p \in \{2, 8\}$.

5.3 Results on selecting the true cluster K

We compared information-criterion-based model selection of the number of clusters for mixture and MoE models using the criteria introduced in Section 4.3: elpd_{loo} and ICL for Bayesian working models, and BIC and ICL for EM working models. Under simulated settings with true $K = 3$ (for data generated from either the mixture model or MoE model), we observed: (i) Bayesian MoE model (**Bayes-MoE**): elpd_{loo} correctly identified $K = 3$ (Table 2). (ii) Bayesian mixture model (**Bayes**): elpd_{loo} shows a mild tendency to favor larger K than the truth. (iii) EM working models (**EM** and **EM-MoE**): BIC correctly identified $K = 3$. Across all settings, ICL was systematically more conservative than the other criteria and preferred smaller K (i.e., slightly under-splitting relative to the truth).

For higher-dimensional ($p = 8$) the mixture and MoE models with true $K = 3$, Supplementary Table S4 indicates that elpd_{loo} shows a mild tendency to favor larger K than the truth for Bayesian working models consistent with the $p = 2$ results, whereas ICL correctly identified $K = 3$ in all scenarios. Similar to the $p = 2$ case, both BIC and ICL from the EM working models (**EM** and **EM-MoE**) correctly identified $K = 3$ across all scenarios, except that **EM** selects $K = 4$ for data generated from the MoE model.

Table 2: Selection of the number of clusters on simulated data generated by the mixture and MoE models with $n = 200$, $p = 2$ and true $K = 3$. Reported are the mean (standard deviation) of each information criterion over 100 simulations. Bayesian working models are evaluated with elpd_{loo} (larger is better) and ICL (smaller is better); EM working models are evaluated with BIC and ICL (both smaller is better). Optimal values per method are bolded.

K	2	3	4	5	6
Data generated by mixture model					
Bayes					
elpd _{loo}	-802.9 (33.5)	-776.2 (33.5)	-775.7 (33.6)	-775.1 (33.5)	-774.6 (33.5)
ICL	1692.0 (70.3)	1753.3 (72.5)	1915.9 (86.5)	2033.3 (85.5)	2143.6 (93.7)
Bayes-MoE					
elpd _{loo}	-1863.5 (33.4)	-1838.6 (33.5)	-1839.0 (33.5)	-1839.0 (33.5)	-1839.2 (33.6)
ICL	4030.0 (63.1)	4158.8 (68.0)	4241.9 (79.6)	4303.5 (85.6)	4383.7 (89.9)
EM					
BIC	3751.5 (66.9)	3725.1 (69.4)	3736.1 (68.2)	3749.7 (68.6)	3766.3 (68.1)
ICL	3796.1 (70.5)	3829.1 (76.2)	3857.9 (73.5)	3869.1 (75.4)	3889.4 (86.1)
EM-MoE					
BIC	3751.9 (67.8)	3720.5 (67.3)	3737.7 (67.9)	3755.3 (67.1)	3772.3 (67.1)
ICL	3797.0 (72.6)	3848.6 (71.8)	3894.5 (80.8)	3932.9 (77.4)	3958.7 (80.3)
Data generated by MoE model					
Bayes					
elpd _{loo}	-830.0 (30.7)	-804.3 (29.5)	-803.8 (29.5)	-803.6 (29.5)	-803.2 (29.5)
ICL	1774.4 (67.6)	1851.7 (62.0)	2024 (71.7)	2152.1 (73.5)	2253.5 (76.0)
Bayes-MoE					
elpd _{loo}	-1850.5 (31.2)	-1812.9 (31.2)	-1813.8 (31.3)	-1814.1 (31.5)	-1815.1 (31.5)
ICL	3902.1 (69.2)	3960.0 (68.7)	4008.5 (70.3)	4061.1 (71.8)	4110.9 (70.2)
EM					
BIC	3821.2 (60.5)	3812.0 (59.9)	3840.7 (58.5)	3874.0 (59.6)	3904.1 (59.3)
ICL	3876.0 (66.3)	3939.0 (63.2)	3979.9 (66.3)	4015.3 (75.6)	4047.5 (78.8)
EM-MoE					
BIC	3734.5 (61.4)	3688.2 (62.4)	3714.9 (62.1)	3741.7 (63.4)	3768.3 (63.7)
ICL	3769.8 (65.6)	3775.3 (64.7)	3822.6 (73.3)	3861.6 (74.6)	3888.4 (77.2)

6 Application to Cancer drug screening data

6.1 Data processing

The Cancer Therapeutics Response Portal (CTRP) v2 is a large-scale cancer cell line drug screening resource comprising responses of 481 compounds across 860 cell lines representing 24 primary tumor types [28]. The data are publicly available at <https://portals.broadinstitute.org/ctrp>. Let $r_i^d(c_j)$ denote the viability (or inhibition) of cell line i ($i = 1, \dots, 860$) at drug concentration/dose c_j with $j = 1, \dots, p$ for drug d , where $d = 1, \dots, 481$. For a given drug d , let n_d be the number of cell lines with measured responses. Let $\mathbf{r}_i^d = (r_i^d(c_1), \dots, r_i^d(c_p))^\top \in \mathbb{R}^p$, and $\bar{\mathbf{r}}^d = (\bar{r}^d(c_1), \dots, \bar{r}^d(c_p))^\top \in \mathbb{R}^p$, where $\bar{r}^d(c_j)$ is the average response at dose c_j across the n_d cell lines with measurements for drug d . The empirical per-drug dose-dose covariance is

$$S^{(d)} = \frac{1}{n_d - 1} \sum_{i=1}^{n_d} (\mathbf{r}_i^d - \bar{\mathbf{r}}^d)(\mathbf{r}_i^d - \bar{\mathbf{r}}^d)^\top \in \mathbb{R}^{p \times p}.$$

This dose-response representation leverages the full dose-response information without reducing it to a single-parameter summary (e.g., IC₅₀ or area under the dose-response curve (AUC); Figure 3) and avoids imposing a specific sigmoid form when curve fitting is unreliable. By modeling covariance across drug dosages, $S^{(d)}$ captures how inhibition at low, intermediate and high doses co-varies across cell lines for each drug, thereby preserving shapes along the dose axis.

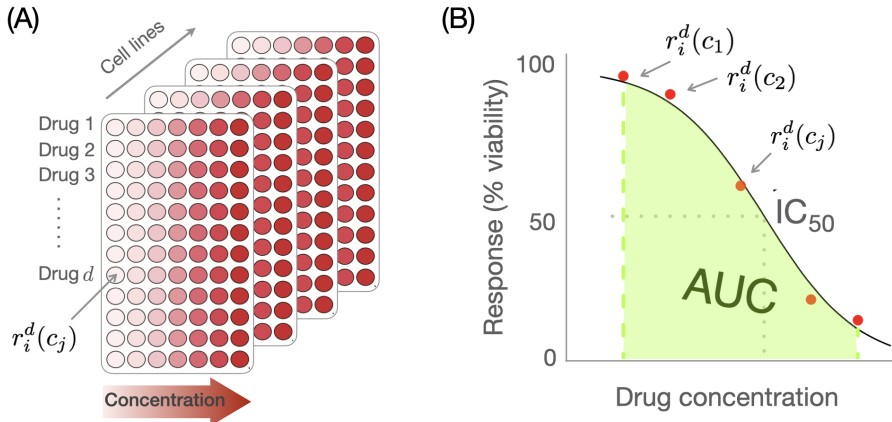


Figure 3: Experimental setup and data for cell lines from patient biopsies treated with drugs at multiple concentrations. (A) Experiment setup for an individual cell line experiment in multi-well cell culture plates. (B) Drug dose/concentration-response relationship for data from one row of wells of the plate. AUC is the area under the dose-response curve, often obtained from a fitted sigmoid function. IC₅₀ (half-maximal inhibitory concentration) represents the concentration of a drug required to reduce cell viability (survival) by 50% compared to a control.

To permit within-drug dose-response covariance estimation, we analyzed a subset of $n = 374$ drugs profiled at the same $p = 5$ concentrations: 0.002, 0.016, 0.130, 1.000 and 8.300 μM . Using replicate viability measurements, we computed one $p \times p$ covariance matrix $S^{(d)}$ per drug, yielding $n = 374$ matrices.

We model the per-drug dose-response covariance matrices using finite mixture and mixture-of-experts models to differentiate latent drug classes. Drugs with similar mechanism-of-action (MoA) are expected to induce similar dose-response shape relationships across cell lines (e.g., how low-, mid- and high-dose effects co-vary); such patterns are encoded in the covariance matrices $S^{(d)}$.

The MoE model formulation additionally accommodates drug- or context-specific covariates (molecular structures and/or genetic information) to sharpen class separation and aid interpretation with respect to molecular targets. For the MoE models, we incorporated two drug-level covariates. The first covariate is drug status, coded as a binary indicator (0: approved by the FDA or used in clinical trials; 1: experimental

compound). The second covariate is derived from the compound SMILES (Simplified Molecular Input Line Entry System), which encodes chemical structure. SMILES strings were converted to molecular fingerprints; we then performed principal component analysis on the fingerprint matrix and used the first principal component as a covariate in the MoE models.

6.2 Results

Model selection results are summarized in Supplementary Table S5. For the Bayesian mixture model (**Bayes**), $K = 5$ and $K = 7$ yield the highest elpd_{loo} values, with $K = 5$ and $K = 7$ essentially tied. The MCMC diagnostics for $K = 5$ (Supplementary Figure S12) indicate stable sampling behavior, and $K = 5$ is also preferred by ICL. Consistent with these findings, the Bayesian MoE model (**Bayes-MoE**) achieves its best elpd_{loo} at $K = 6$, but $K = 5$ yields comparable predictive performance (Supplementary Table S5), stable MCMC behavior (Supplementary Figure S13), and is favored by ICL. We therefore use $K = 5$ for both Bayesian methods in subsequent analyses. In contrast, the EM-based mixture and MoE models selected $K = 10$ and $K = 11$, respectively, under both BIC/ICL (see Supplementary Table S5).

To assess whether the drug groupings produced by the four methods are biologically meaningful, we validated them against well-annotated mechanisms of action (MoA) curated for the same compounds. As a baseline, we also compared with hierarchical clustering of drug sensitivity profiles using the area under the dose-response curve (AUC), a common practice in the literature [28, 37, 36, 35]. We restricted the comparison to 172 drugs assayed across 370 cell lines with complete AUC measurements. Visual inspection of the dendrogram derived from the standardized AUC values (complete linkage method with Euclidean distance; Figure 4) indicates that the AUC-based clustering yields groupings that are largely inconsistent with established MoAs and tends to mix agents with disparate targets and pharmacology.

In contrast, the **Bayes-MoE** model produced clusters that coherently align with biologically interpretable MoAs (purity= 0.490, Figure 5). We quantify MoA coherence using cluster purity, defined as the fraction of compounds aligned with the majority MoA within each cluster (see the caption of Figure 5 for the exact formula). Notably, receptor tyrosine kinase (RTK) inhibitors are consolidated into the same cluster under the **Bayes-MoE** model for many agents: sunitinib, nilotinib, linifanib, tandutinib, NVP-ADW742, KW-2449 and SU11274. This concordance spans multiple RTK classes (e.g., VEGFRs, c-KIT, FLT3), reflecting the shared target class and expected pharmacodynamic similarity. For cytotoxic DNA-damaging agents and alkylators, **Bayes-MoE** similarly aggregates platinum compounds and classical alkylators into coherent clusters consistent with their common MoA: temozolomide, bendamustine, carboplatin and organoplatinum Platin. While the Bayesian mixture model (**Bayes**) often produced similar high-level groupings (purity= 0.480, Figure 5), it exhibited inconsistencies for several MoAs. For example, histone deacetylase (HDAC) inhibitors were split across multiple clusters under **Bayes**: vorinostat, belinostat and entinostat — despite sharing a primary target class (HDAC1/2/3/6/8). Likewise, classical antimetabolites and nucleoside analogs spanned multiple clusters: methotrexate, gemcitabine, cytarabine, clofarabine and nelarabine, fragmenting a pharmacologically coherent MoA class.

The EM-based methods (**EM** and **EM-MoE**) were even less stable with respect to MoA coherence (purity 0.334 and 0.295, respectively; Figure 5). For example, RTK inhibitors were scattered across multiple clusters by **EM**, and **EM-MoE** assignments further split the same set of RTK agents across several groups. These observations underscore the advantage of **Bayes-MoE** in capturing modular structure aligned with mechanism-informed biological classes. Figure 6 shows the posterior means of the covariance matrices corresponding to the five components.

7 Discussion and conclusion

This work develops a unified framework for clustering covariance matrix data. By formulating a fully Bayesian mixture of Wishart distributions and extending it to a mixture-of-experts architecture, we move beyond mean-based clustering paradigms and directly model variability in covariance patterns. This

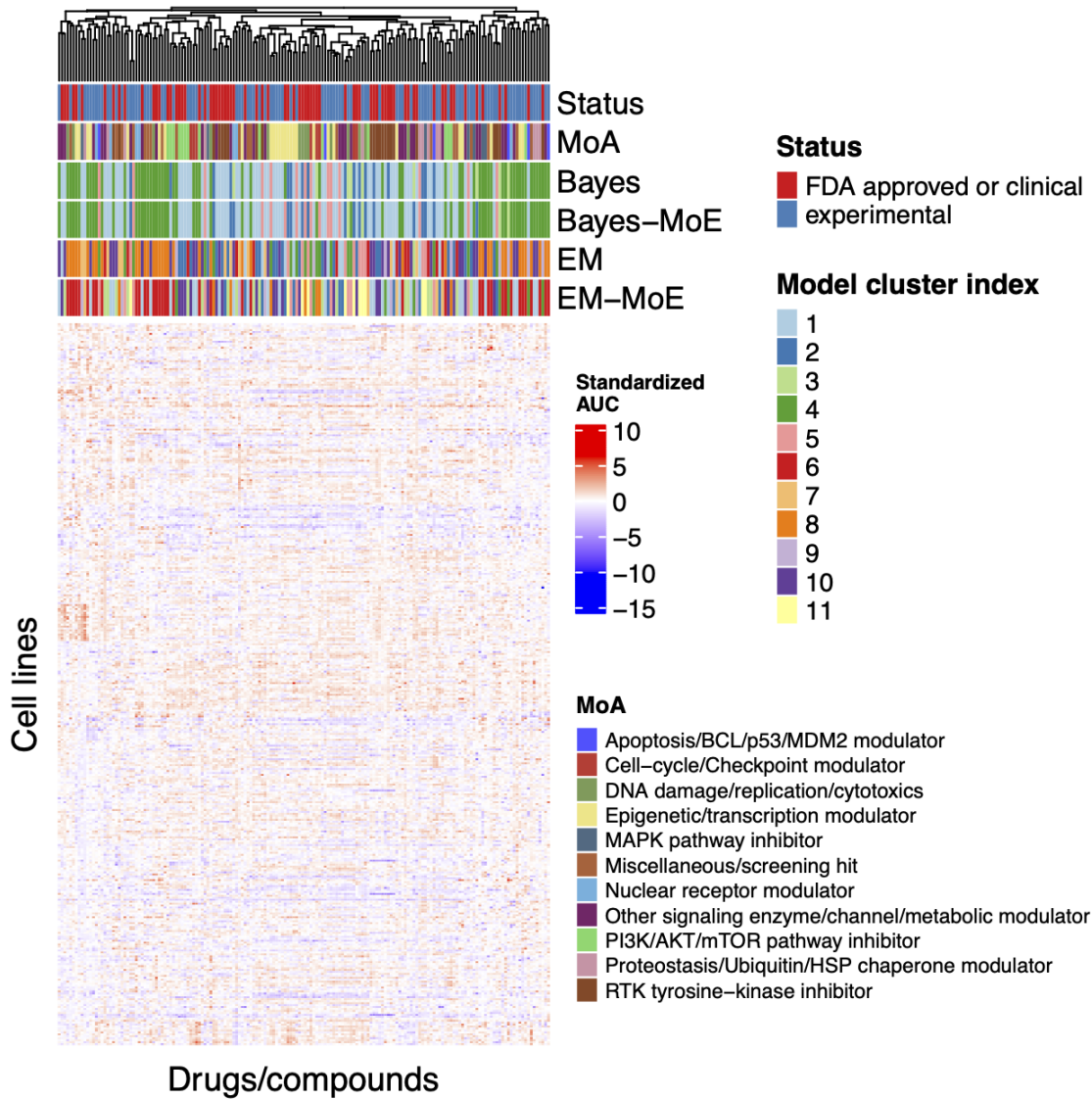


Figure 4: Drug clustering based on sensitivity data. The heatmap shows AUC values for 370 cell lines treated with 172 drugs. AUCs were standardized and subjected to hierarchical clustering (complete linkage method with Euclidean distance) to assess similarity among compounds. The legend “Model cluster index” shows the cluster labels from the four methods. As shown, AUC-derived clusters are not aligned with known mechanism-of-actions (**MoA**), whereas the Bayesian MoE model yields more coherent mechanism-based groupings.

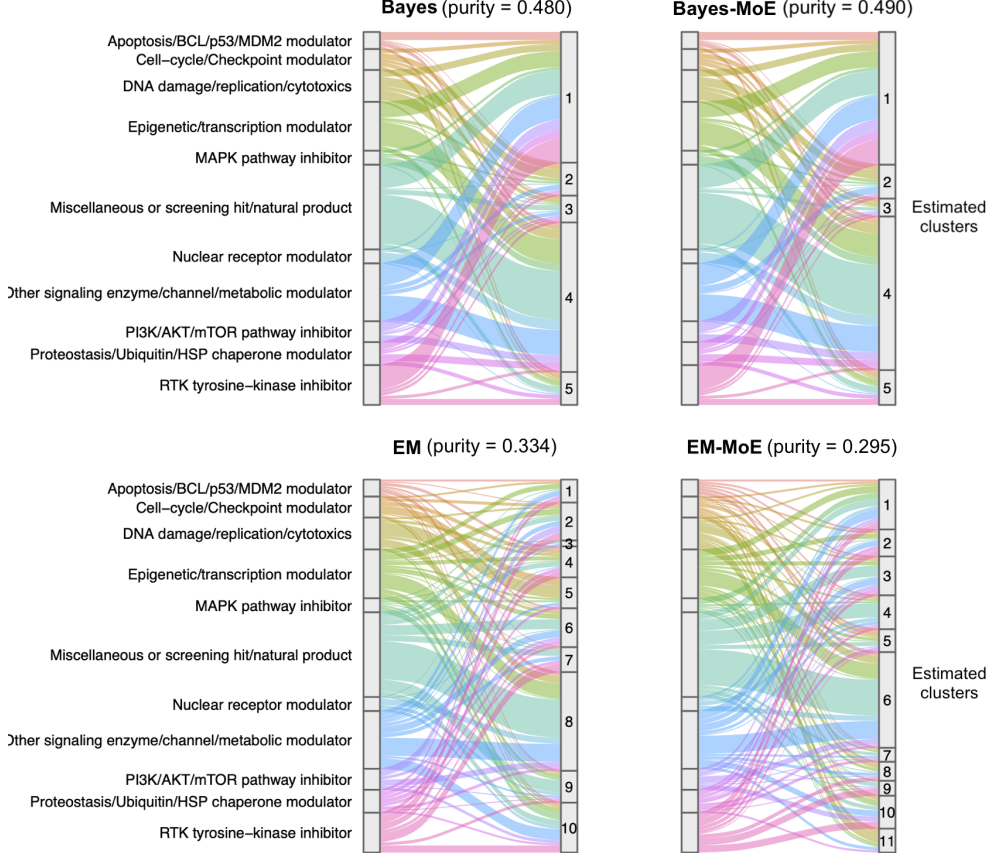


Figure 5: Alluvial diagrams showing flows from MoA groups into individual model-based clusters, illustrating cluster-MoA cohesion. Purity in each panel is defined as: $\text{purity} = \frac{1}{n} \sum_{k=1}^K \max_c |\{i : \text{cluster}(i) = k \wedge \text{MoA_group}(i) = c\}|$.

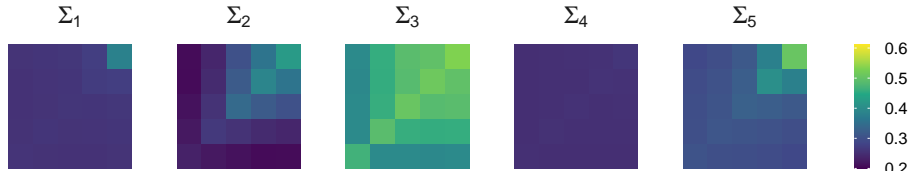


Figure 6: Heatmaps of the posterior mean covariance matrices estimated by **Bayes-MoE** on the cancer drug screening data with $K = 5$.

perspective is particularly well suited to scientific settings in which dependence structures themselves are the primary objects of interest, such as financial co-movements, functional connectivity in neuroscience, and drug dose-response relationships in pharmacology.

A key contribution of the proposed MoE-Wishart model lies not only in its ability to accommodate covariate-dependent clustering through a probabilistic gating network, but also in the development of tailored inference algorithms that make such modeling practically feasible. By allowing mixing proportions to vary with observed predictors, the model captures systematic changes in latent covariance regimes while maintaining interpretability and flexibility beyond standard mixtures with fixed weights. To support this structure, we develop specialized MCMC algorithms that respect the geometry of symmetric positive definite matrices and yield stable posterior inference, as well as a novel EM procedure for maximum

likelihood estimation in the mixture-of-experts setting where closed-form updates are unavailable. Across simulations and real-data applications, this combination of model design and algorithmic innovation leads to improved stability and inferential coherence relative to existing EM-based approaches.

In the cancer drug screening analysis, modeling full dose–dose covariance descriptors preserved rich information on how drug effects co-vary across concentrations and enabled more meaningful drug stratification than scalar summarized descriptor such as AUC. Among all methods considered, the Bayesian MoE–Wishart model with $K = 5$ clusters achieved stable model fit and produced clusters that aligned closely with curated biochemical mechanisms of drug action, coherently grouping RTK inhibitors and DNA-damaging or alkylating agents according to their shared pharmacology. In contrast, EM-based mixture approaches yielded fragmented and biologically inconsistent groupings. These results demonstrate that jointly modeling drug dose–response covariance structure and drug-level covariates within a Bayesian MoE framework provides a robust and interpretable approach for uncovering mechanism-informed drug classes in large-scale screening data.

Several limitations point to promising directions for future research. First, the Wishart likelihood imposes restrictive assumptions on covariance structure, such as unimodality and limited tail behavior, which may be inadequate in settings with extreme dependence patterns or heavy-tailed variability. Extensions to more flexible matrix-variate distributions or nonparametric Bayesian mixtures could alleviate these constraints. Second, scalability remains a challenge for very high-dimensional covariance matrices or large numbers of components, motivating the development of more efficient sampling schemes or variational approximations. Finally, richer gating networks—potentially incorporating nonlinear or hierarchical covariate effects—could further enhance the expressiveness of the MoE–Wishart framework and broaden its applicability to increasingly complex structured data. Theoretical properties would also be the objective of future works [15, 18, 17, 16, 14, 13].

Although the MoE framework incorporates covariates at the covariance-descriptor level, it abstracts away individual-level information (e.g., patient-specific clinical or genomic covariates). One natural extension is supervised hierarchical Gaussian process (GP) functional regression, where covariates govern the mean and a GP captures smoothness over the input domain, coupled with residual covariance modeling (e.g., Wishart) and the latent clusters to encode subpopulations similarity. Alternatively, mixtures can be placed directly on GPs, for example, using spectral mixture kernels [22], mixtures of GPs [31], or mixtures of GP experts [25], to model multimodal, heterogeneous functional responses with complex covariate effects.

Acknowledgments

The views, findings, and opinions presented in this work are exclusively those of the author and do not reflect the official stance of the Norwegian Institute of Public Health. Z.Z. was supported by the ERA PerMed under the ERA-NET Cofund scheme of the European Union’s Horizon 2020 research and innovation framework program (grant ‘SYMMETRY’ ERA-PERMED2021-330).

Conflicts of interest/Competing interests

The authors declare no potential conflict of interests.

References

- [1] Ashburn, T. T. and Thor, K. B. (2004). Drug repositioning: identifying and developing new uses for existing drugs. *Nature Reviews Drug Discovery*, 3(8):673–683.
- [2] Biernacki, C., Celeux, G., and Govaert, G. (2002). Assessing a mixture model for clustering with the integrated completed likelihood. *IEEE transactions on pattern analysis and machine intelligence*, 22(7):719–725.

- [3] Cappozzo, A. and Casa, A. (2025). Model-based clustering for covariance matrices via penalized Wishart mixture models. *Computational Statistics & Data Analysis*, 212:108232.
- [4] Chaudhari, N., Mitra, S. K., Chirakkal, S., Mandal, S., Putrevu, D., and Misra, A. (2021). Discrimination of multi-crop scenarios with polarimetric SAR data using Wishart mixture model. *Journal of Applied Remote Sensing*, 15(3):034514–034514.
- [5] Frühwirth-Schnatter, S., Celeux, G., and Robert, C. P. (2019). *Handbook of mixture analysis*. CRC press.
- [6] Gallaugher, M. P. and McNicholas, P. D. (2018). Finite mixtures of skewed matrix variate distributions. *Pattern Recognition*, 80:83–93.
- [7] Gao, H., Zhang, T., Wu, Y., Jiang, L., Zhan, J., Li, J., and Yang, R. (2014). Multiple-trait genome-wide association study based on principal component analysis for residual covariance matrix. *Heredity*, 113(6):526–532.
- [8] Hidot, S. and Saint-Jean, C. (2010). An Expectation–Maximization algorithm for the Wishart mixture model: Application to movement clustering. *Pattern Recognition Letters*, 31(14):2318–2324.
- [9] Huang, K., Lalagkas, P. N., Sultan, B., and Melamed, R. (2025). Exploiting similarity in drug molecular effects for drug repurposing. *Human Genomics*, 19:110.
- [10] Jiang, W. and Tanner, M. A. (1999). On the identifiability of mixtures-of-experts. *Neural Networks*, 12(9):1253–1258.
- [11] Johansson, K., Ogut, M. G., Pelger, M., Schmelzer, T., Boyd, S., et al. (2023). A simple method for predicting covariance matrices of financial returns. *Foundations and Trends® in Econometrics*, 12(4):324–407.
- [12] Jordan, M. I. and Jacobs, R. A. (1994). Hierarchical mixtures of experts and the EM algorithm. *Neural computation*, 6(2):181–214.
- [13] Mai, T. T. (2024a). Concentration of a Sparse Bayesian Model With Horseshoe Prior in Estimating High-Dimensional Precision Matrix. *Stat*, 13(4):e70008.
- [14] Mai, T. T. (2024b). High-dimensional sparse classification using exponential weighting with empirical hinge loss. *Statistica Neerlandica*, 78(4):664–691.
- [15] Mai, T. T. (2025a). Concentration properties of fractional posterior in 1-bit matrix completion. *Machine Learning*, 114(1):7.
- [16] Mai, T. T. (2025b). Handling bounded response in high dimensions: a horseshoe prior bayesian beta regression approach. *arXiv preprint arXiv:2505.22211*.
- [17] Mai, T. T. (2025c). High-dimensional Bayesian Tobit regression for censored response with Horseshoe prior. *arXiv preprint arXiv:2505.08288*.
- [18] Mai, T. T. (2025d). On properties of fractional posterior in generalized reduced-rank regression. *Journal of Multivariate Analysis*, page 105481.
- [19] Mai, T. T., Rønneberg, L., Zhao, Z., Zucknick, M., and Corander, J. (2019). Learning cancer drug sensitivities in large-scale screens from multi-omics data with local low-rank structure. In *International Meeting on Computational Intelligence Methods for Bioinformatics and Biostatistics*, pages 67–79. Springer.

- [20] Nguyen, H. D. and Chamroukhi, F. (2018). Practical and theoretical aspects of mixture-of-experts modeling: An overview. *Wiley Interdisciplinary Reviews: Data Mining and Knowledge Discovery*, 8(4):e1246.
- [21] Nielsen, S. F., Madsen, K. H., Schmidt, M. N., and Mørup, M. (2017). Modeling dynamic functional connectivity using a Wishart mixture model. In *2017 International Workshop on Pattern Recognition in Neuroimaging (PRNI)*, pages 1–4. IEEE.
- [22] Parra, G. and Tobar, F. (2017). Spectral mixture kernels for multi-output Gaussian processes. In *Proceedings of the 31st International Conference on Neural Information Processing Systems*, NIPS’17, page 6684–6693, Red Hook, NY, USA. Curran Associates Inc.
- [23] Peng, F., Jacobs, R. A., and Tanner, M. A. (1996). Bayesian inference in mixtures-of-experts and hierarchical mixtures-of-experts models with an application to speech recognition. *Journal of the American Statistical Association*, 91(435):953–960.
- [24] Quandt, R. E. and Ramsey, J. B. (1978). Estimating mixtures of normal distributions and switching regressions. *Journal of the American statistical Association*, 73(364):730–738.
- [25] Rasmussen, C. and Ghahramani, Z. (2001). Infinite mixtures of Gaussian process experts. In Dietterich, T., Becker, S., and Ghahramani, Z., editors, *Advances in Neural Information Processing Systems*, volume 14. MIT Press.
- [26] Runcie, D. E. and Mukherjee, S. (2013). Dissecting high-dimensional phenotypes with Bayesian sparse factor analysis of genetic covariance matrices. *Genetics*, 194(3):753–767.
- [27] Schäfer, J. and Strimmer, K. (2005). A shrinkage approach to large-scale covariance matrix estimation and implications for functional genomics. *Statistical applications in genetics and molecular biology*, 4(1):32.
- [28] Seashore-Ludlow, B., Rees, M. G., Cheah, J. H., Cokol, M., Price, E. V., Coletti, M. E., Jones, V., Bodycombe, N. E., Soule, C. K., Gould, J., Alexander, B., Li, A., Montgomery, P., Wawer, M. J., Kuru, N., Kotz, J. D., Hon, C. S.-Y., Munoz, B., Liefeld, T., Dančík, V., Bittker, J. A., Palmer, M., Bradner, J. E., Shamji, A. F., Clemons, P. A., and Schreiber, S. L. (2015). Harnessing connectivity in a large-scale small-molecule sensitivity dataset. *Cancer Discovery*, 5(11):1210–1223.
- [29] Sharifi-Noghabi, H., Jahangiri-Tazehkand, S., Smirnov, P., Hon, C., Mammoliti, A., Nair, S. K., Mer, A. S., Ester, M., and Haibe-Kains, B. (2021). Drug sensitivity prediction from cell line-based pharmacogenomics data: guidelines for developing machine learning models. *Briefings in Bioinformatics*, 22(6):bbab294.
- [30] Sun, R., Ma, T., Liu, S., and Sathye, M. (2019). Improved covariance matrix estimation for portfolio risk measurement: A review. *Journal of Risk and Financial Management*, 12(1):48.
- [31] Tresp, V. (2000). Mixtures of Gaussian processes. In Leen, T., Dietterich, T., and Tresp, V., editors, *Advances in Neural Information Processing Systems*, volume 13. MIT Press.
- [32] Tuzel, O., Porikli, F., and Meer, P. (2006). Region covariance: A fast descriptor for detection and classification. In Leonardis, A., Bischof, H., and Pinz, A., editors, *Computer Vision – ECCV 2006*, page 589–600. Springer Berlin Heidelberg.
- [33] Vehtari, A., Gelman, A., and Gabry, J. (2017). Practical Bayesian model evaluation using leave-one-out cross-validation and WAIC. *Statistics and Computing*, 27(5):1413–1432.

- [34] Xue, H., Li, J., Xie, H., and Wang, Y. (2018). Review of drug repositioning approaches and resources. *International Journal of Biological Sciences*, 14(10):1232–1244.
- [35] Zeng, A. G. X., Bansal, S., Jin, L., Mitchell, A., Chen, W. C., Abbas, H. A., Chan-Seng-Yue, M., Voisin, V., van Galen, P., Tierens, A., Cheok, M., Preudhomme, C., Dombret, H., Daver, N., Futreal, P. A., Minden, M. D., Kennedy, J. A., Wang, J. C. Y., and Dick, J. E. (2022). A cellular hierarchy framework for understanding heterogeneity and predicting drug response in acute myeloid leukemia. *Nature Medicine*, 28(6):1212–1223.
- [36] Zhao, Z., Wang, S., Zucknick, M., and Aittokallio, T. (2022). Tissue-specific identification of multi-omics features for pan-cancer drug response prediction. *iScience*, 25(8):104767.
- [37] Zhao, Z. and Zucknick, M. (2020). Structured penalized regression for drug sensitivity prediction. *Journal of the Royal Statistical Society Series C: Applied Statistics*, 69(3):525–545.

A Details on Algorithm

In Section 3.1 Gibbs-within-MH sampler for mixture model, we can integrate out $\boldsymbol{\pi}$ in Eq (6):

$$\begin{aligned}
& p(z_i = k \mid z_{-i}, S_i, \{\Sigma_\ell, \nu_\ell\}, \boldsymbol{\alpha}) \\
& \propto \int \pi_k f_{\mathcal{W}}(S_i \mid \nu_k, \Sigma_k) \cdot \text{Dir}(\boldsymbol{\pi} \mid z_{-i}, \boldsymbol{\alpha}) d\boldsymbol{\pi} \\
& \propto \int \pi_k f_{\mathcal{W}}(S_i \mid \nu_k, \Sigma_k) \cdot \text{Dir}(\boldsymbol{\pi} \mid \boldsymbol{\alpha}) \cdot \text{Cat}(z_{-i} \mid \boldsymbol{\alpha}) d\boldsymbol{\pi} \\
& \propto \int \pi_k f_{\mathcal{W}}(S_i \mid \nu_k, \Sigma_k) \cdot \text{Dir}(\boldsymbol{\pi} \mid \boldsymbol{a}) d\boldsymbol{\pi}, \text{ where } a_j = \alpha_j + n_{-i,j}, n_{-i,j} := \#\{l \neq i \mid z_l = j\} \\
& = f_{\mathcal{W}}(S_i \mid \nu_k, \Sigma_k) \int \pi_k \prod_{j=1}^K \frac{\pi_j^{a_j-1}}{B(\boldsymbol{a})} d\boldsymbol{\pi} \\
& = f_{\mathcal{W}}(S_i \mid \nu_k, \Sigma_k) \frac{1}{B(\boldsymbol{a})} \int \pi_1^{a_1-1} \pi_2^{a_2-1} \cdots \pi_k^{a_k-1} \cdots \pi_K^{a_K-1} d\boldsymbol{\pi} \\
& = f_{\mathcal{W}}(S_i \mid \nu_k, \Sigma_k) \frac{1}{B(\boldsymbol{a})} B(a_1, \dots, a_k + 1, \dots, a_K) \int d\mathbb{P}_{\boldsymbol{\pi} \sim \text{Dir}(a_1, \dots, a_k + 1, \dots, a_K)} \\
& = f_{\mathcal{W}}(S_i \mid \nu_k, \Sigma_k) \cdot a_k / \sum_{j=1}^K a_j \\
& \propto f_{\mathcal{W}}(S_i \mid \nu_k, \Sigma_k) \cdot (\alpha_k + n_{-i,k})
\end{aligned}$$

This induces better MCMC mixing than sampling from the conditional distribution in Eq (6).

B Additional simulation results

Table S3: Effective sample sizes (ESS) for the mixture and mixture-of-experts working models. Data are generated from the mixture-of-experts model. Reported are the means (standard deviations) of ESS over 100 simulations for selected parameters. ν_1 and ν_2 are the degrees of freedom of the Wishart distributions for the first two clusters. $\Sigma_{1,11}$ and $\Sigma_{2,11}$ are the (1, 1)-entries of the corresponding scale matrices. β_{11} and β_{12} are the drug-status effects for the first two clusters.

Working model	ν		Σ		β	
	ν_1	ν_2	$\Sigma_{1,11}$	$\Sigma_{2,11}$	β_{11}	β_{12}
Mixture model: $p = 2$						
$n = 200$	723 (203)	169 (53)	1179 (435)	216 (78)	-	-
$n = 500$	784 (113)	169 (37)	1243 (343)	214 (54)	-	-
$n = 1000$	790 (124)	169 (28)	1155 (317)	200 (40)	-	-
Mixture model: $p = 8$						
$n = 200$	1397 (92)	722 (57)	8885 (743)	3222 (426)	-	-
$n = 500$	1484 (72)	814 (54)	8908 (829)	3591 (304)	-	-
$n = 1000$	1450 (85)	761 (49)	9495 (639)	3453 (346)	-	-
MoE model: $p = 2$						
$n = 200$	996 (168)	251 (75)	1289 (483)	313 (120)	133 (71)	131 (75)
$n = 500$	1023 (103)	223 (43)	1366 (345)	263 (57)	164 (40)	203 (71)
$n = 1000$	1009 (82)	233 (38)	1438 (312)	271 (52)	179 (53)	187 (48)
MoE model: $p = 8$						
$n = 200$	1342 (90)	752 (53)	8644 (1009)	3333 (368)	407 (106)	418 (111)
$n = 500$	1495 (78)	814 (47)	8843 (449)	3475 (416)	442 (84)	446 (91)
$n = 1000$	1458 (82)	796 (44)	9514 (871)	3588 (329)	469 (108)	439 (83)

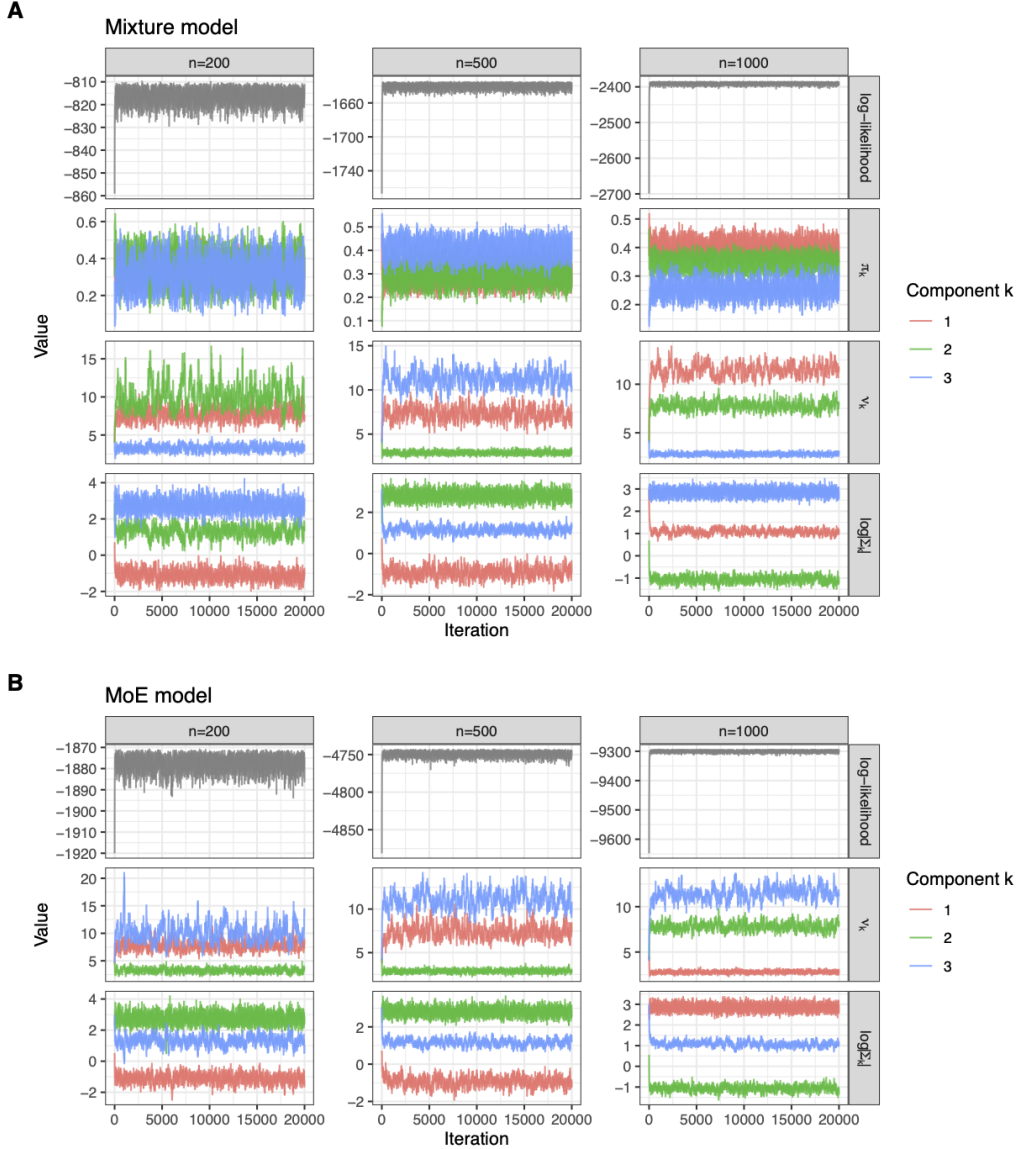


Figure S7: Trace plots for MCMC diagnosis for simulated data generated by the **mixture model** with $p = 2$ and $n = (200, 500, 1000)$, fitted by the Bayesian mixture and MoE working models. (A) MCMC diagnosis for the mixture model fit. For each n , diagnosis is for the model's log-likelihood, π_k , ν_k and $\log|\Sigma_k|$, $k \in \{1, 2, 3\}$. (B) MCMC diagnosis for the MoE model fit. For each n , diagnosis is for the model's log-likelihood, ν_k and $\log|\Sigma_k|$, $k \in \{1, 2, 3\}$.

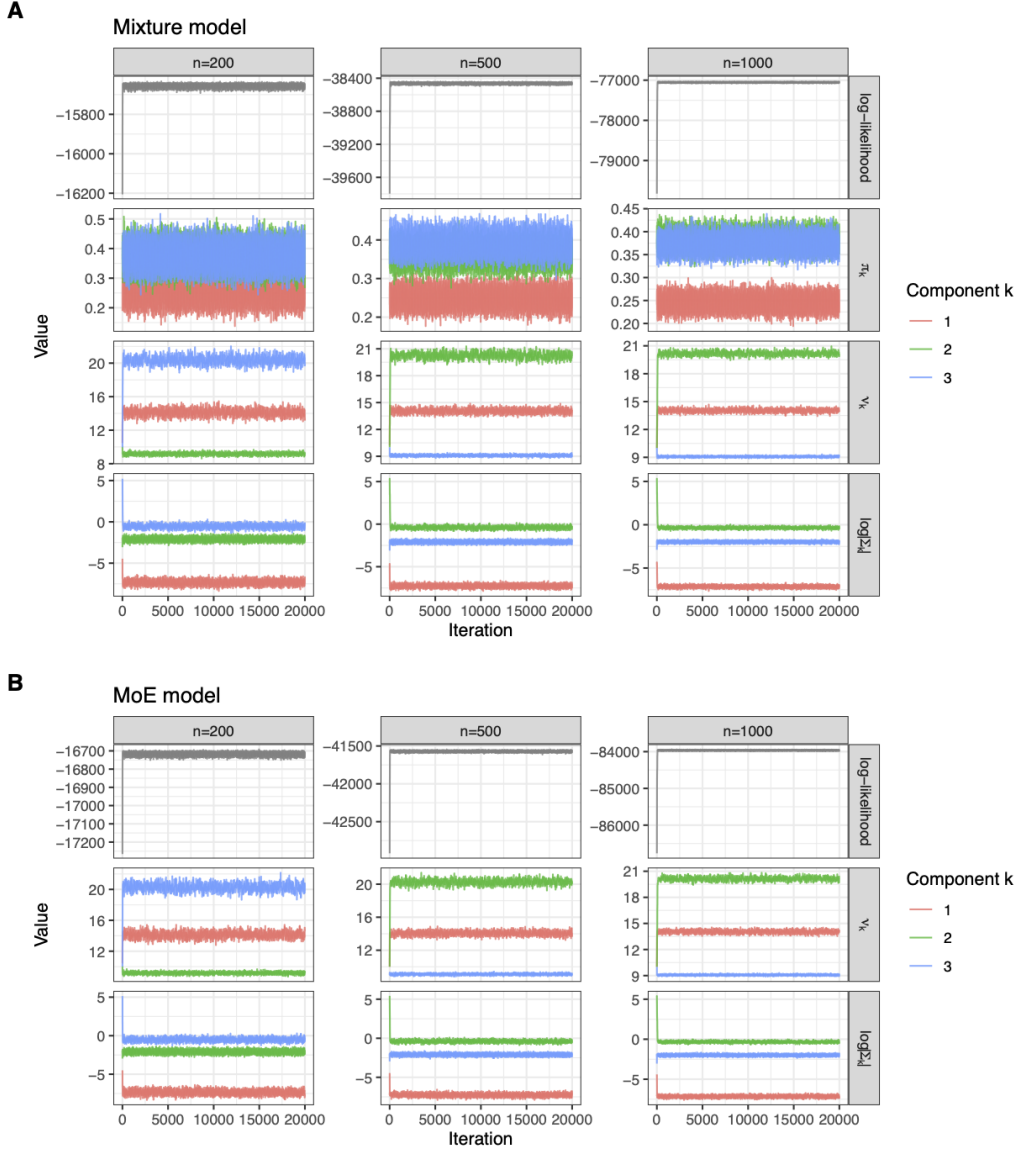


Figure S8: Trace plots for MCMC diagnosis for simulated data generated by the **mixture model** with $p = 8$ and $n = (200, 500, 1000)$, fitted by the Bayesian mixture and MoE working models. (A) MCMC diagnosis for the mixture model fit. For each n , diagnosis is for the model's log-likelihood, π_k , ν_k and $\log |\Sigma_k|$, $k \in \{1, 2, 3\}$. (B) MCMC diagnosis for the MoE model fit. For each n , diagnosis is for the model's log-likelihood, ν_k and $\log |\Sigma_k|$, $k \in \{1, 2, 3\}$.

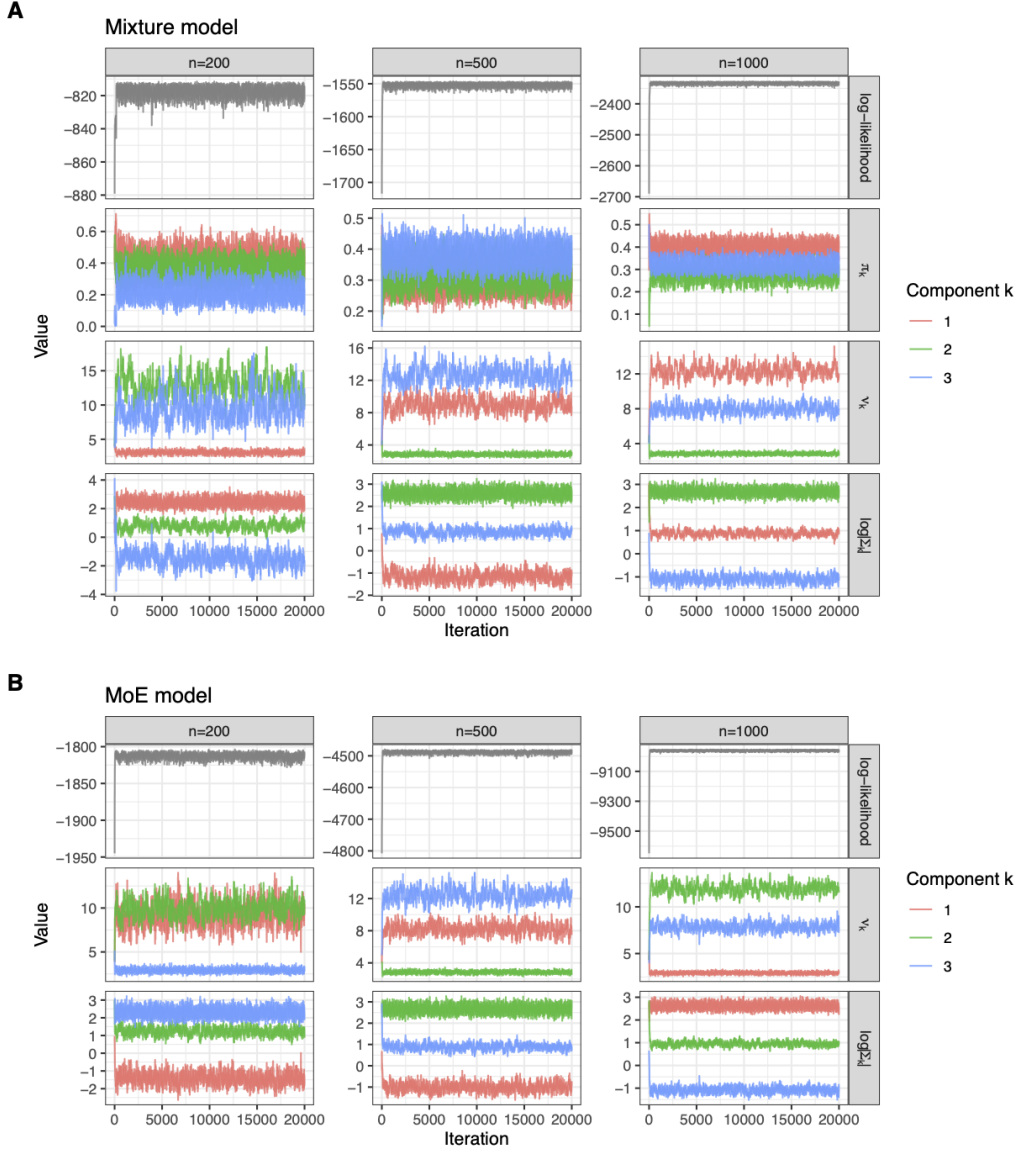


Figure S9: Trace plots for MCMC diagnosis for simulated data generated by the **MoE model** with $p = 2$ and $n = (200, 500, 1000)$, fitted by the Bayesian mixture and MoE working models. (A) MCMC diagnosis for the mixture model fit. For each n , diagnosis is for the model's log-likelihood, π_k , ν_k and $\log |\Sigma_k|$, $k \in \{1, 2, 3\}$. (B) MCMC diagnosis for the MoE model fit. For each n , diagnosis is for the model's log-likelihood, ν_k and $\log |\Sigma_k|$, $k \in \{1, 2, 3\}$.

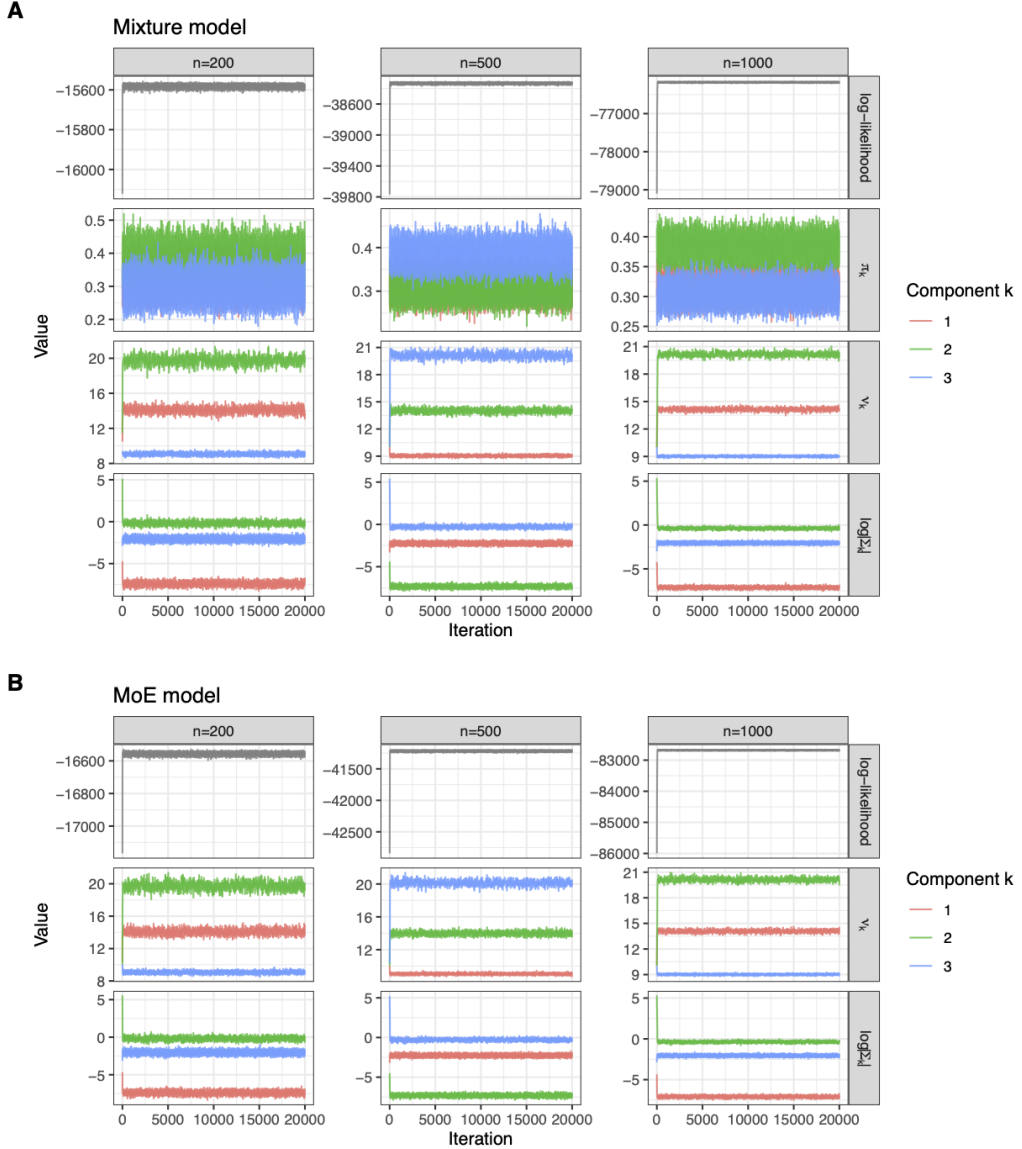


Figure S10: Trace plots for MCMC diagnosis for simulated data generated by the **MoE model** with $p = 8$ and $n = (200, 500, 1000)$, fitted by the Bayesian mixture and MoE working models. (A) MCMC diagnosis for the mixture model fit. For each n , diagnosis is for the model's log-likelihood, π_k , ν_k and $\log|\Sigma_k|$, $k \in \{1, 2, 3\}$. (B) MCMC diagnosis for the MoE model fit. For each n , diagnosis is for the model's log-likelihood, ν_k and $\log|\Sigma_k|$, $k \in \{1, 2, 3\}$.

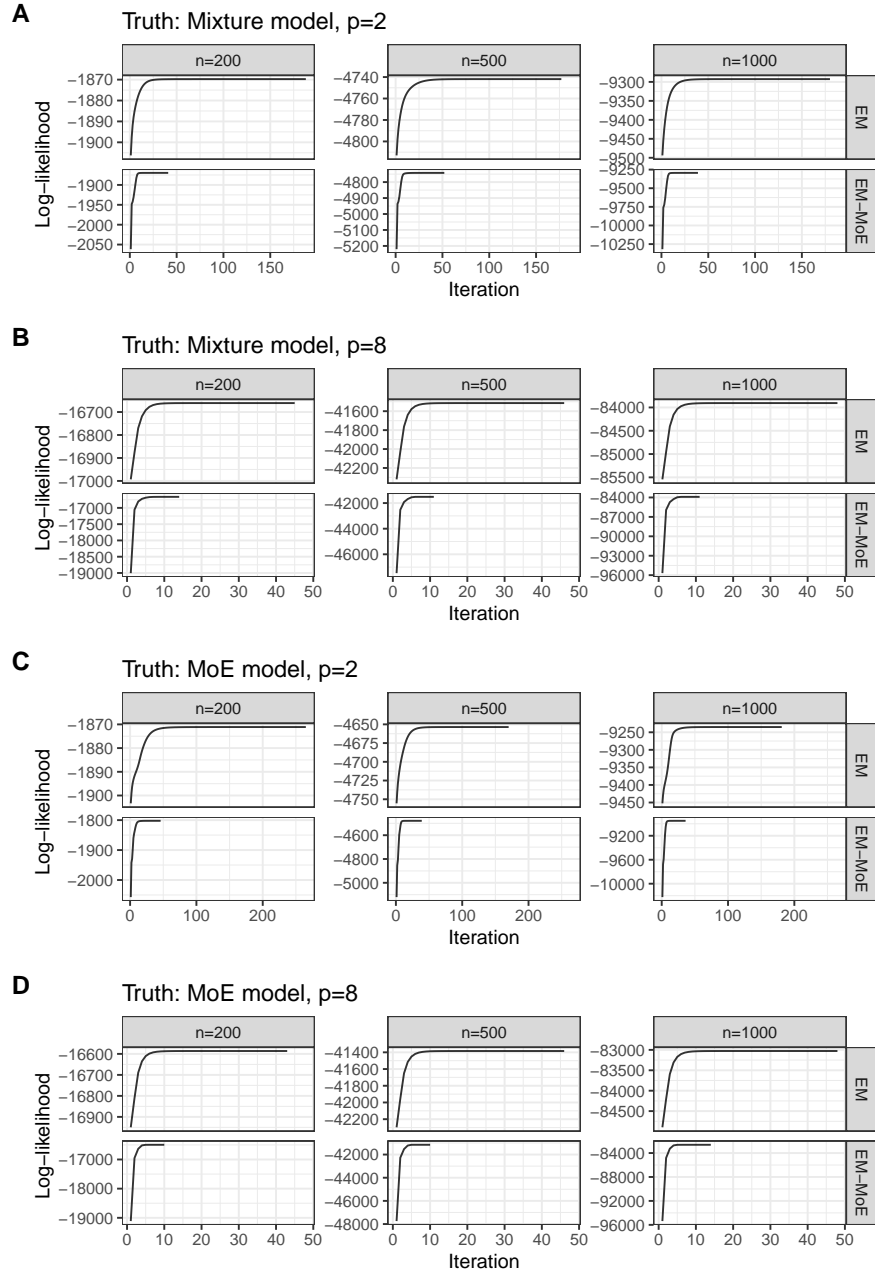


Figure S11: The log-likelihood per iteration by EM algorithms for simulated data generated from the mixture or MoE models (truth). Each of panels (A)-(D) has columns for simulated data $n = (200, 500, 1000)$, and has rows for mixture and MoE model fits (EM and EM-MoE, respectively). (A) The true underlying model is a mixture model with dimension $p = 2$. (B) The true underlying model is a mixture model with dimension $p = 8$. (C) The true underlying model is a MoE model with dimension $p = 2$. (D) The true underlying model is a MoE model with dimension $p = 8$.

Table S4: Simulation results on selection of the number of clusters. Data are generated by the mixture and MoE models with $n = 1000$, $p = 8$ and true $K = 3$. Reported are the mean (standard deviation) of each information criterion over 100 simulations. Bayesian working models are evaluated with elpd_{loo} (larger is better) and ICL (smaller is better); EM working models are evaluated with BIC and ICL (both smaller is better). Optimal values per method are bolded.

K	2	3	4	5	6
Data generated by mixture model					
Bayes					
elpd _{loo}	-78662.4 (544.7)	-77428.5 (577.6)	-77428.4 (577.6)	-77428.0 (577.7)	-77427.3 (577.6)
ICL	157764.8 (1089.5)	155549.2 (1154.5)	155810.7 (1154.5)	156070.2 (1155.2)	156329.8 (1155.3)
Bayes-MoE					
elpd _{loo}	-85571.1 (544.6)	-84338.2 (577.6)	-84330.3 (577.2)	-84325.7 (577.0)	-84320.5 (577.7)
ICL	172927.5 (1101.1)	171499.7 (1145.8)	171729.0 (1145.6)	171961.5 (1144.7)	172196.3 (1144.5)
EM					
BIC	171506.3 (1089.4)	169254.8 (1121.0)	169338.1 (1157.6)	169481.5 (1159.5)	169514.5 (1171.1)
ICL	171506.4 (1089.5)	169276.4 (1120.2)	169382.0 (1157.4)	169564.3 (1156.5)	169586.0 (1168.8)
EM-MoE					
BIC	171506.4 (1089.4)	169230.8 (1155.3)	169420.4 (1155.2)	169616.6 (1151.3)	169802.9 (1155.2)
ICL	171506.4 (1089.5)	169252.6 (1154.6)	169538.4 (1176.7)	169794.1 (1164.0)	170196.2 (1191.2)
Data generated by MoE model					
Bayes					
elpd _{loo}	-77825.9 (508.9)	-76470.2 (537.1)	-76470.1 (537.1)	-76469.8 (537.0)	-76469.8 (537.0)
ICL	156111.9 (1017.9)	153674.1 (1073.9)	153956.7 (1074.0)	154238.1 (1073.8)	154521.5 (1074.1)
Bayes-MoE					
elpd _{loo}	-84432.7 (506.4)	-82973.6 (538.2)	-82968.6 (538.4)	-82963.9 (537.4)	-82958.0 (537.2)
ICL	170048.4 (1020.5)	168002.7 (1073.5)	168249.6 (1073.8)	168503.4 (1072.3)	168751.4 (1072.0)
EM					
BIC	169853.4 (1017.9)	167874.3 (1490.0)	167500.0 (1135.3)	167628.5 (1104.8)	167769.9 (1080.3)
ICL	169853.4 (1017.9)	167892.0 (1483.6)	167537.7 (1133.4)	167694.8 (1120.2)	167851.0 (1085.3)
EM-MoE					
BIC	169243.1 (1013.0)	166530.6 (1076.6)	166735.7 (1075.0)	166957.3 (1073.0)	167152.2 (1073.2)
ICL	169243.1 (1012.9)	166548.0 (1076.7)	166835.1 (1085.4)	167112.3 (1089.0)	167491.9 (1089.9)

C Additional results on drug response data analysis

Table S5: Selection of the number of clusters K on cancer drug response data. Bayesian methods (**Bayes** and **Bayes-MoE**) are evaluated with elpd_{loo} (larger is better) and ICL (smaller is better). EM methods (**EM** and **EM-MoE**) are evaluated with BIC and ICL (both smaller is better). Optimal values per method are bolded.

K	2	3	4	5	6	7	8	9	10	11
Bayes										
elpd _{loo}	8269.6	9369.8	9507.2	9700.2	9696.9	9700.4	9698.7	-	-	-
ICL	-16371	-18461.6	-18628.7	-18892.5	-18775.6	-18670.7	-18554.1			
Bayes-MoE										
elpd _{loo}	6054.9	7158.1	7283.5	7463.4	7466.0	7462.2	7465.1	-	-	-
ICL	-11560.8	-13324.8	-13397.9	-13549.6	-13438.6	-13316.6	-13202.9	-	-	-
EM										
BIC	-12156.4	-15347.2	-16034.7	-16591.1	-16769	-17365.2	-17508.3	-17359.9	-17742.7	-17595.2
ICL	-12139.3	-15335.2	-16007.3	-16555.2	-16728.2	-17336.9	-17473.2	-17328.8	-17704.9	-17555.8
EM-MoE										
BIC	-12167.3	-15369.4	-15927.1	-16646.1	-17102.4	-17374.4	-17516.8	-17768.2	-17810.3	-17874.0
ICL	-12150.3	-15357.5	-15900.4	-16614.8	-17072.1	-17343	-17479.6	-17731.4	-17770.0	-17839.7

Table S6: Additional results on cancer drug sensitivity real data. Parameter estimation by four competing methods. The two mixture models are **Bayes** (with $K = 5$ clusters) and **EM** (with $K = 10$ clusters). The two MoE models are **Bayes-MoE** (with $K = 5$ clusters) and **EM-MoE** (with $K = 11$ clusters), and included two concomitant covariates: (i) drug status coded as a binary variable and (ii) the first principal component from PCA of the drug SMILES-derived fingerprint matrix. Selected parameters are reported with point estimates by **EM** and **EM-MoE** methods, and with posterior means (95% credible interval) by **Bayes** and **Bayes-MoE**. ν_1 and ν_2 are the first two clusters' Wishart distributions' degrees of freedom. $\Sigma_{1,11}$ and $\Sigma_{2,11}$ are the first two clusters' Wishart distributions' scale matrices' first entries. π_1 and π_2 are the first two clusters' mixture weights. β_{11} and β_{12} are the first two clusters' drug status' effects.

Parameter	Bayes	EM	Bayes-MoE	EM-MoE
ν_1	10.9 (10.3, 11.4)	31.4	10.8 (10.3, 11.4)	33.6
ν_2	12.4 (11.0, 13.9)	37.2	12.4 (10.9, 14.0)	24.5
$\Sigma_{1,11}$	0.3 (0.24, 0.28)	0.09	0.3 (0.24, 0.28)	0.08
$\Sigma_{2,11}$	0.2 (0.19, 0.28)	0.08	0.2 (0.19, 0.28)	0.11
π_1	0.4 (0.32, 0.42)	0.06	β_{11}	-0.2 (-0.87, 0.51)
π_2	0.1 (0.05, 0.11)	0.10	β_{12}	-1.0 (-2.01, 0.05)
				-0.34

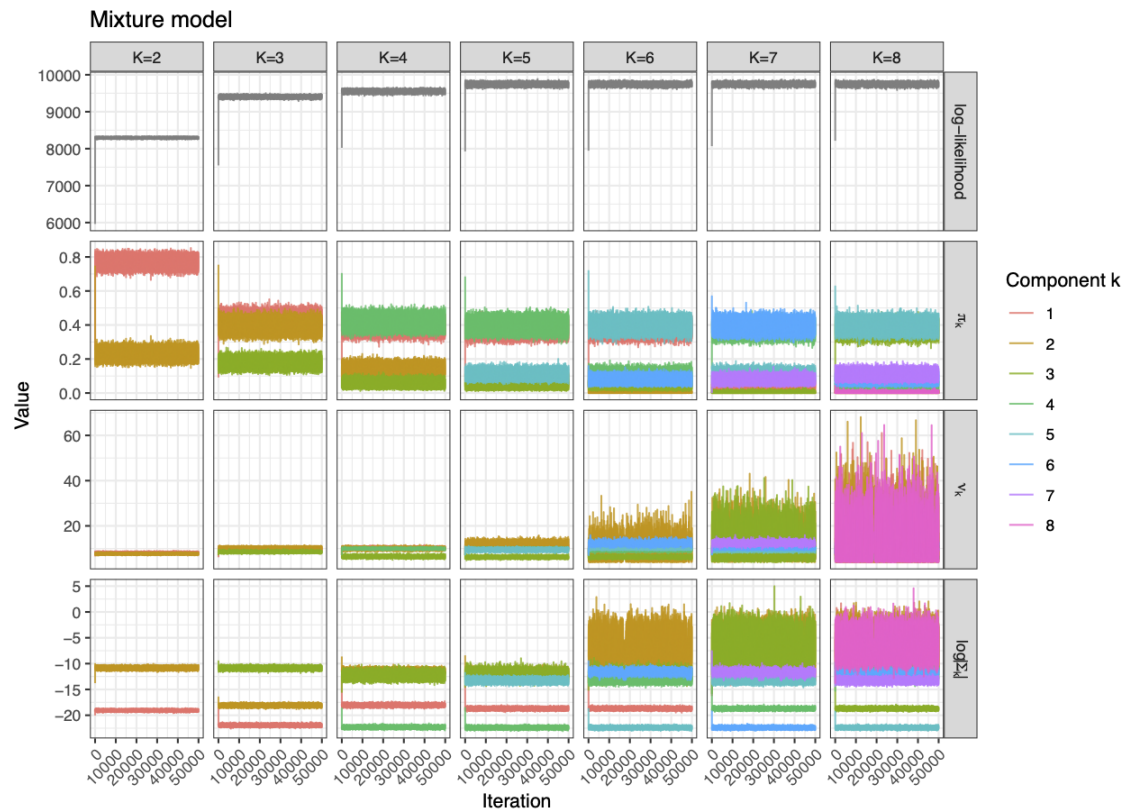


Figure S12: Additional results on cancer drug sensitivity real data. Trace plots for MCMC diagnostics of parameters for drug sensitivity data fitted by the **mixture model** with specified $K \in \{2, 3, 4, 5, 6, 7, 8\}$. The first row shows the trace plots of the model's log-likelihood with respect to K . The second row shows the trace plots of π_k (mixture weight), $k = 1, 2, \dots, K$, with respect to K . The third row shows the trace plots of ν_k (Wishart distribution's degree of freedom) with respect to K . The fourth row shows the trace plots of $\log|\Sigma_k|$ (Σ_k is the Wishart distribution's scale matrix) with respect to K . The legend shows different colors for component/cluster index k .

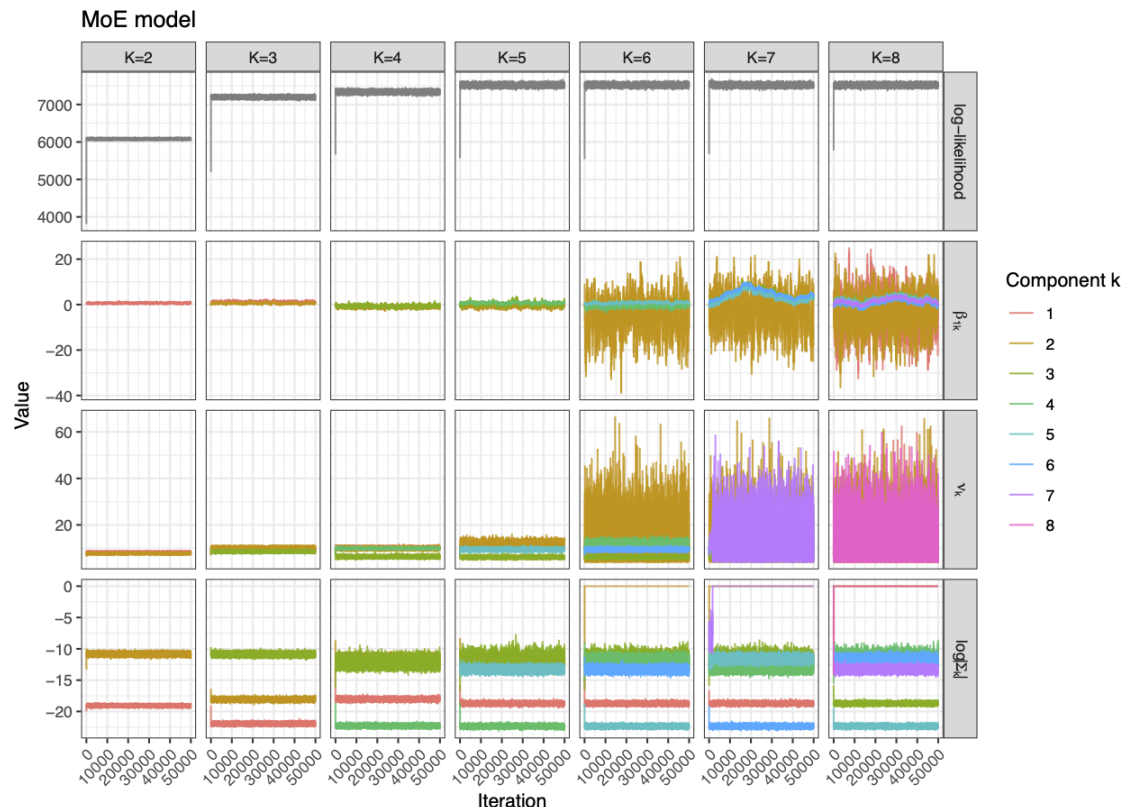


Figure S13: Additional results on cancer drug sensitivity real data. Trace plots for MCMC diagnostics of parameters for drug sensitivity data fitted by the **mixture-of-experts model** with specified $K \in \{2, 3, 4, 5, 6, 7, 8\}$. The first row shows the trace plots of the model's log-likelihood with respect to K . The second row shows the trace plots of β_{1k} (drug-status effect), $k = 1, 2, \dots, K$, with respect to K . The third row shows the trace plots of ν_k (Wishart distribution's degree of freedom) with respect to K . The fourth row shows the trace plots of $\log |\Sigma_k|$ (Σ_k is the Wishart distribution's scale matrix) with respect to K . The legend shows different colors for component/cluster index k .